Department of
Industry and Resources

RECORD
2005/7

REGOLITH–LANDFORM MAPPING AND HYPERSPECTRAL DATA FOR THE KALGOORLIE–KANOWNA AREA

by M. Skwarnecki

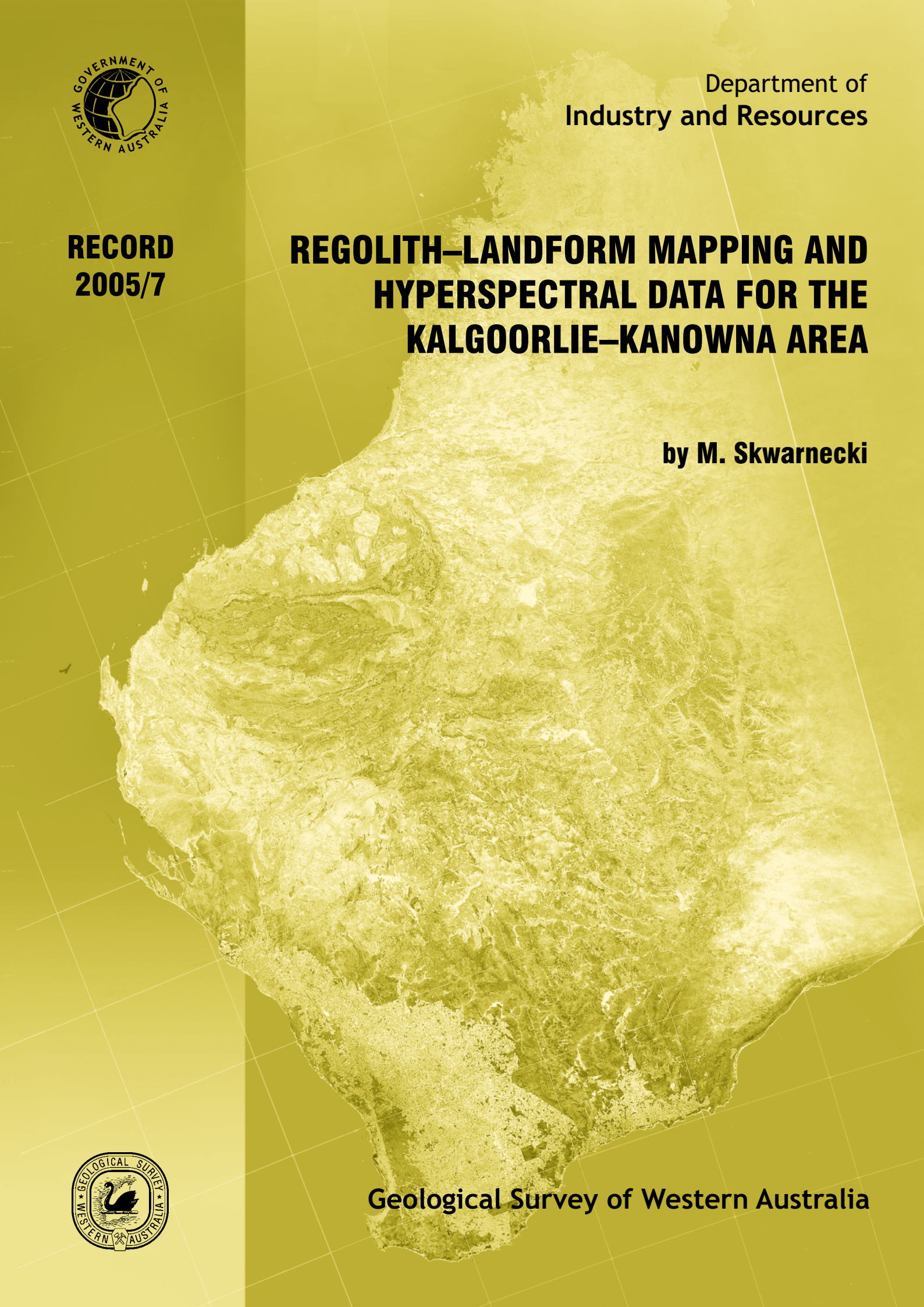

Geological Survey of Western Australia

GEOLOGICAL SURVEY OF WESTERN AUSTRALIA

Record 2005/7

REGOLITH–LANDFORM MAPPING AND HYPERSPECTRAL DATA FOR THE KALGOORLIE–KANOWNA AREA

by
M. Skwarnecki

Perth 2005

MINISTER FOR STATE DEVELOPMENT
Hon. Alan Carpenter MLA

DIRECTOR GENERAL, DEPARTMENT OF INDUSTRY AND RESOURCES
Jim Limerick

DIRECTOR, GEOLOGICAL SURVEY OF WESTERN AUSTRALIA
Tim Griffin

REFERENCE
The recommended reference for this publication is:
SKWARNECKI, M., 2005, Regolith–landform mapping and hyperspectral data for the Kalgoorlie–Kanowna area: Western Australia Geological Survey, Record 2005/7, 49p.

National Library of Australia Card Number and ISBN 1 74168 008 5

Grid references in this publication refer to the Geocentric Datum of Australia 1994 (GDA94). Locations mentioned in the text are referenced using Map Grid Australia (MGA) coordinates, Zone 51. All locations are quoted to at least the nearest 5 m.

Cover image modified from Landsat data, courtesy of ACRES

Published 2005 by Geological Survey of Western Australia
This Record is published in digital format (PDF), as part of a digital dataset on CD, and is available online at www.doir.wa.gov.au/gswa/onlinepublications. Laser-printed copies can be ordered from the Information Centre for the cost of printing and binding.

Further details of geological publications and maps produced by the Geological Survey of Western Australia are available from:
Information Centre
Department of Industry and Resources
100 Plain Street
EAST PERTH, WESTERN AUSTRALIA 6004
Telephone: +61 8 9222 3459 Facsimile: +61 8 9222 3444
www.doir.wa.gov.au/gswa/onlinepublications

Contents

Appendices

Figures

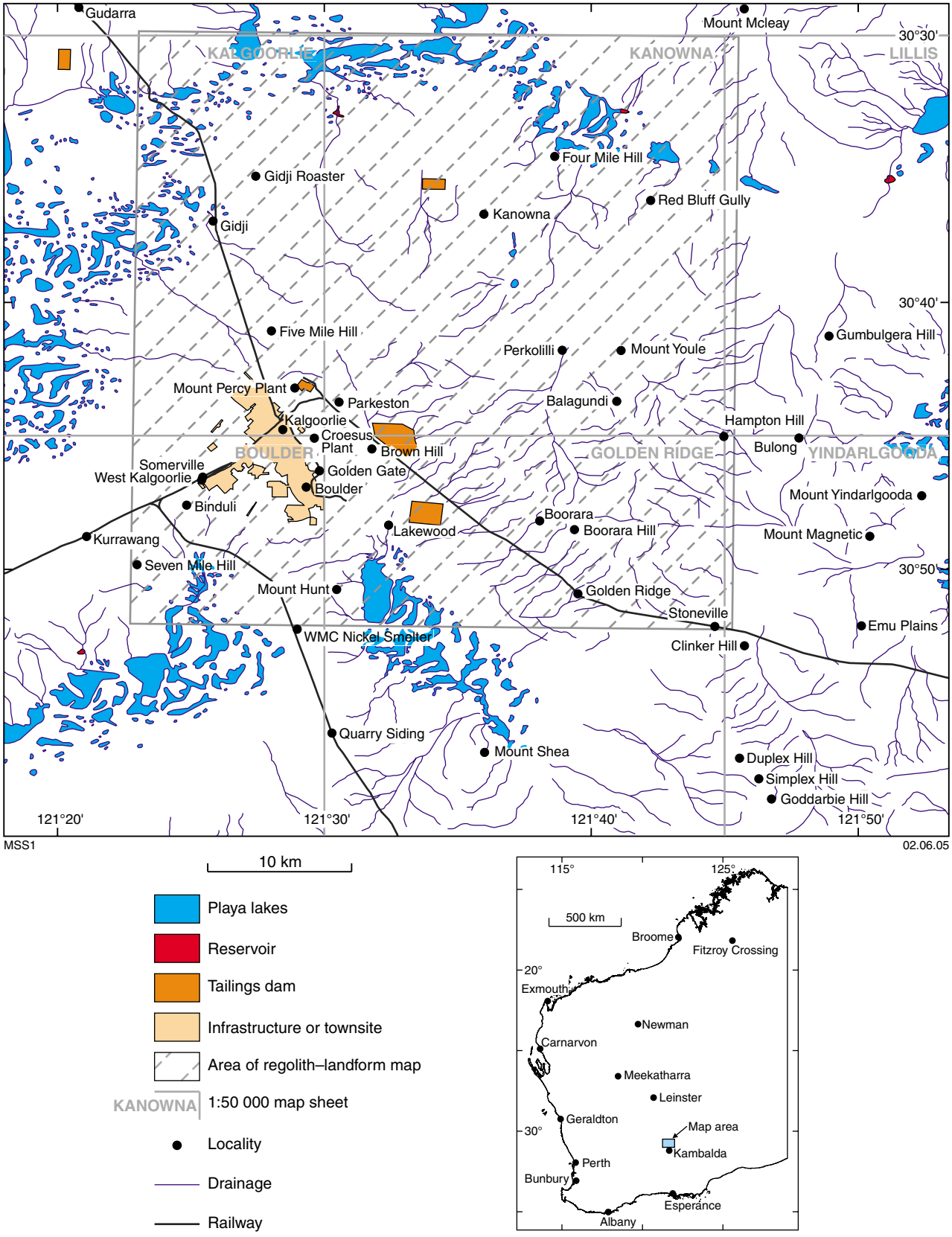

Figure 1. Locality map showing the area of the Kalgoorlie–Kanowna regolith–landform map

Regolith–landform mapping and hyperspectral data for the Kalgoorlie–Kanowna area

by

M. Skwarnecki

Abstract

Two principal regolith–landform domains were identified in the Kalgoorlie–Kanowna area: a dominant colluvial–relict domain, and a less common surrounding eolian–playa domain overlying alluvial deposits. Within these domains, regolith–landform units can be assigned to eight primary categories: residual or relict (*R*), exposed (*X*), colluvial (*C*), low-gradient slope (*W*), alluvial (*A*), lacustrine (*L*), eolian (*E*), and sandplain (*S*). Examples from each category are described. Knowledge of regolith–landform domains can assist in selecting appropriate exploration geochemical sampling techniques. Airborne hyperspectral data acquired for the region in association with CSIRO, HyVista Corporation, Placer Dome, and MERIWA is another dataset providing additional insight into the nature and evolution of the regolith.

KEYWORDS: regolith, landforms, mapping, Kalgoorlie, Kanowna, Western Australia

Introduction

Most regolith–landform maps show the distribution of regolith materials qualified by landform information (e.g. Craig and Anand, 1993), commonly following the relict–erosional–depositional (RED) scheme of Anand et al. (1993), or the RTMAP approach of Pain et al. (1991), where regolith composition is the primary classifier and landform is secondary. Gozzard (2004) used a different approach to map the regolith–landforms of the Kalgoorlie–Kanowna area, using landform as the primary identifier and composition as a qualifier, following the Geological Survey of Western Australia (GSWA) scheme of Hocking et al. (2001).

Regolith–landform mapping of the Kalgoorlie area commenced in 2001–02 as part of the Development Areas Resource Mapping (DARM) project of GSWA. The object of the DARM program is to undertake detailed regolith–landform mapping and resource delineation in regional areas of Western Australia that are likely to undergo significant development, and where land use planning would benefit from the availability of digital and hardcopy geoscience datasets. Available digital datasets for the area of KALGOORLIE*, BOULDER, KANOWNA, and GOLDEN RIDGE (including 1:25 000 digital orthophotography, Landsat TM images, magnetic (TMI) and Bouguer gravity images, regolith–landform field observations, abandoned mine sites data, and mine and mineral deposits (MINEDEX) data) were released in 2004 (GSWA, 2004). During 2004 regolith–landform mapping of KALGOORLIE and BOULDER was reassessed and fieldwork was completed for KANOWNA and GOLDEN RIDGE. These notes describe the regolith–landform map at 1:50 000 scale presented as a layer in the digital dataset. Digital mineral coverages on DVD, derived from hyperspectral data, complement the regolith–landform map. The HyMap™ metadata are shown in Appendix 1. The 1:100 000 Kalgoorlie–Kanowna hyperspectral mineral map (Cudahy et al., 2005a) is also on DVD. This Record describes regolith–landform mapping of the Kalgoorlie–Kanowna area.

* Capitalized names refer to standard 1:50 000 map sheets, unless otherwise indicated.

Location

The mapped area (Fig. 1) straddles the eastern margin of KALGOORLIE and the western margin of KURNALPI 1:100 000 sheets, over KANOWNA, and eastern, northeastern, and northern parts respectively of KALGOORLIE, BOULDER, and GOLDEN RIDGE.

Previous regolith–landform mapping in the Kalgoorlie district

The first systematic mapping of regolith in the Kalgoorlie region was carried out by Kriewaldt (1974) as part of the geological mapping of KALGOORLIE 1:250 000 sheet

(Kriewaldt, 1969). Kriewaldt divided the regolith into six units (in order of decreasing age):

a) old alluvium: kaolinitic clays locally with horizons of sandstone (with angular quartz), and hematite-cemented sandstone and conglomerate;

b) old weathering products and deposits: sand and loam, locally with ferruginous nodules, ferruginous gravel in a ferruginous clay matrix, indurated ferruginous materials, and silcrete;

c) deposits with 'epigenetic limestone': loams with calcrete nodules, hardpans, ferruginous gravel with a calcareous cement, and calcrete-cemented detritus;

d) alluvium: dominantly sandy to silty alluvium with clays and, locally, gravel;

e) gypsiferous and related deposits: gypsiferous sheets and dunes, and sands and silts with 'crumbly' calcrete; and

f) youngest materials: playa and playa-margin deposits, pediment veneers (lag), eolian-sand deposits, and claypan deposits.

Chan et al. (1988, 1992) produced a 1:1 000 000-scale regolith terrain map of the southeastern part of the Yilgarn Craton, including the Kalgoorlie area. Using remotely sensed data such as Landsat-5 Multispectral Scanner (MSS) and Thematic Mapper (TM), National Oceanic and Atmospheric Administration (NOAA) Advanced Very High Resolution Radiometer (AVHRR) imagery, and Nimbus-7 Coastal Zone Colour Scanner (CZCS), they defined 59 units on the basis of recurring associations of regolith and landforms (using geology, geomorphology, soils, topography, vegetation, and land systems). Limited fieldwork was carried out to validate their interpretations. Aspects of the landscape history and regolith around Kalgoorlie were discussed by Ollier et al. (1988).

Craig and Anand (1993) produced a 1:250 000-scale regolith–landform map for the Kalgoorlie–Kurnalpi area on the basis of the RED scheme. Their units were based on regolith composition and qualified by landform. More-detailed mapping was carried out around Kanowna (Dell, 1992; Ladhams, 1994) using the RED approach. Riganti et al. (2003) reinterpreted the regolith of the Eastern Goldfields and produced a seamless regolith map, using Landsat TM, previously published 1:100 000-scale maps, and limited field checking.

Methodology

Regolith–landform polygons were interpreted in ArcMap onto a rectified orthophotograph base with an overlay of height contours at 0.5 m intervals derived from the digital elevation model. The GSWA regolith classification system (Hocking et al., 2001), based on landform position and regolith composition, was used to code the polygons. As digital databases have taken on more importance, GSWA has developed a system for unambiguous database storage of map codes. Databases cannot store certain character types (including subscripted codes), and some codes are used in both regolith and lithostratigraphic nomenclature (e.g. 'A' is both a primary regolith code and an Archaean age qualifier in lithological coding). To distinguish a regolith code from a lithostratigraphic code, the former is prefixed by an underbar ('_'), and non-subscripted codes are prefaced by a hyphen ('-'). For example, iron-rich alluvium is coded in the database as _A-f (i.e. *Af* on regolith maps), whereas an alluvial fan deposit is coded as _Af (i.e. A_f). Appendix 2 lists the regolith map code and its corresponding database code.

Supporting digital datasets included Landsat TM (Tapley and Gozzard, 1992), HyMap™ (Cudahy et al., 2005a,b), and field observations from the GSWA corporate database (WAROX). The map was produced as a digital product nominally at 1:25 000 scale, with digitizing of individual polygons at 1:5 000 scale. Field validation (during 2004) consisted of traverses along roads, tracks, and major grid lines across the mapped area; 1085 sites were described.

Regolith–landform units

Two principal regolith–landform domains are present in the mapped area (Fig. 2). The larger (colluvial–relict) domain is characterized by low hills and rises (commonly with outcrops of weathered to almost fresh bedrock). Away from the main areas of outcrop, locally sourced colluvium overlies saprolite, which forms pediment. In this report, the term 'pediment' is used for a gently inclined to level landform of generally low relief downslope from adjacent hills with markedly steeper slopes, and is broadly equivalent to peneplain (Eggleton, 2001). The term 'rejuvenated pediment' is used to describe a younger landform, commonly bounded by breakaways, cut into the older pediment. A veneer (typically <2 m thick) of eolian or alluvial material may also overlie saprolite, and these areas are also included within the pediment. The broad pediment is fringed by a transitional zone, where a mantle of variable thickness (but normally <25 m) of transported material, sits above saprolite. The eolian–playa domain, which overlies dominantly alluvial deposits (interpreted as a relict fluvial system), fringes the more extensive colluvial–relict domain.

Within the two domains, regolith–landform units can be assigned to eight primary landform categories (Fig. 3): residual or relict (*R*); exposed (*X*); colluvial (*C*); low-gradient slope (*W*); alluvial (*A*); lacustrine (*L*); eolian (*E*); and sandplain (*S*). Three anthropogenic categories (mining; gravel pit or quarry; infrastructure) are also included on the map.

Colluvial–relict domain

The principal components of this domain are ranges of low hills and rises surrounded by a gently inclined to flat pediment. The low hills are incised by major northerly or northwesterly drainages and northeasterly to southwesterly tributaries. Secondary (rejuvenated) pediments, typically fringed by breakaways, may be cut into the older pediment by this drainage system. The

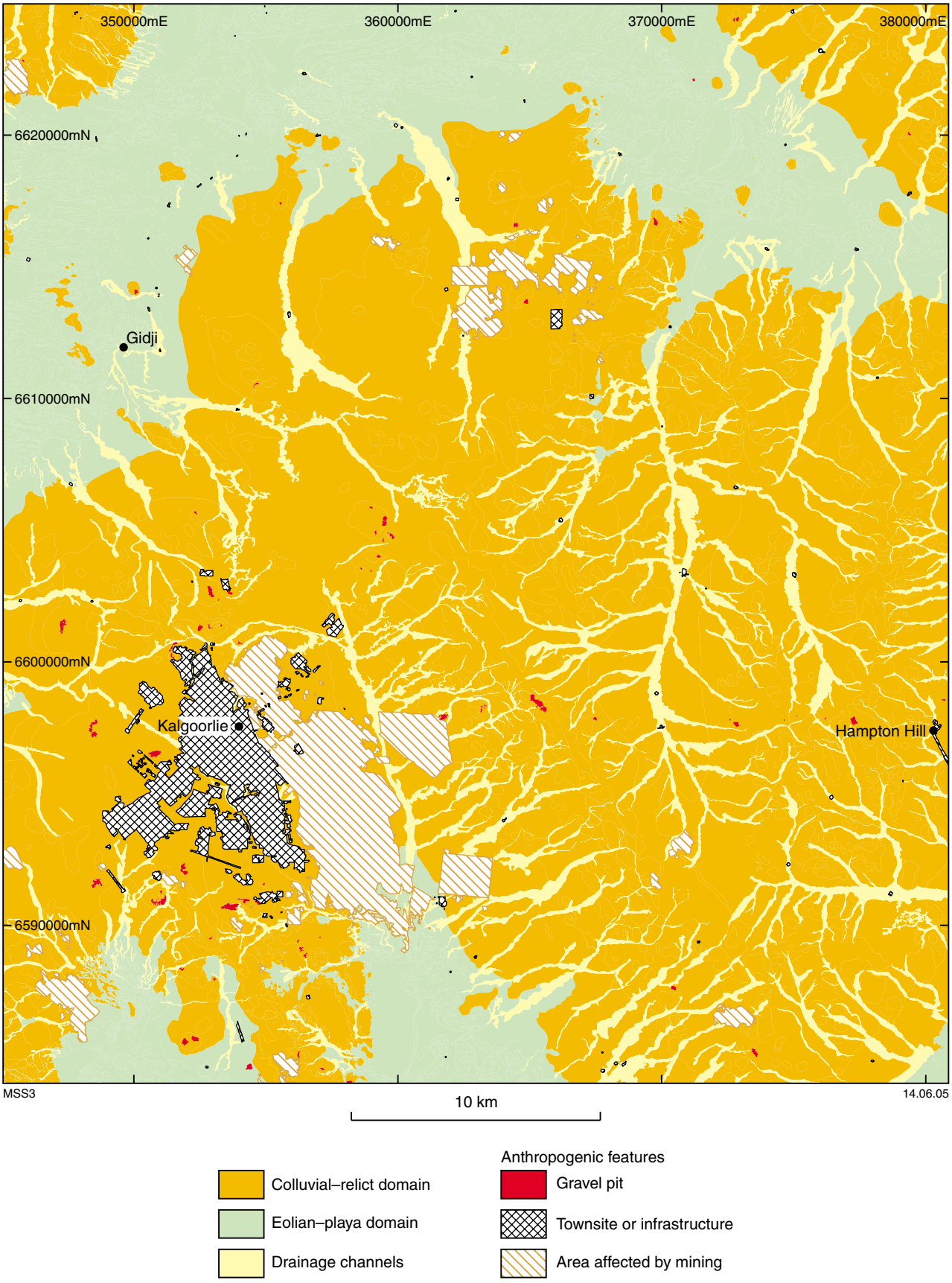

Figure 2. Distribution of the two principal regolith–landform domains (colluvial–relict domain and eolian–playa domain). Drainages cut across the boundaries of both domains

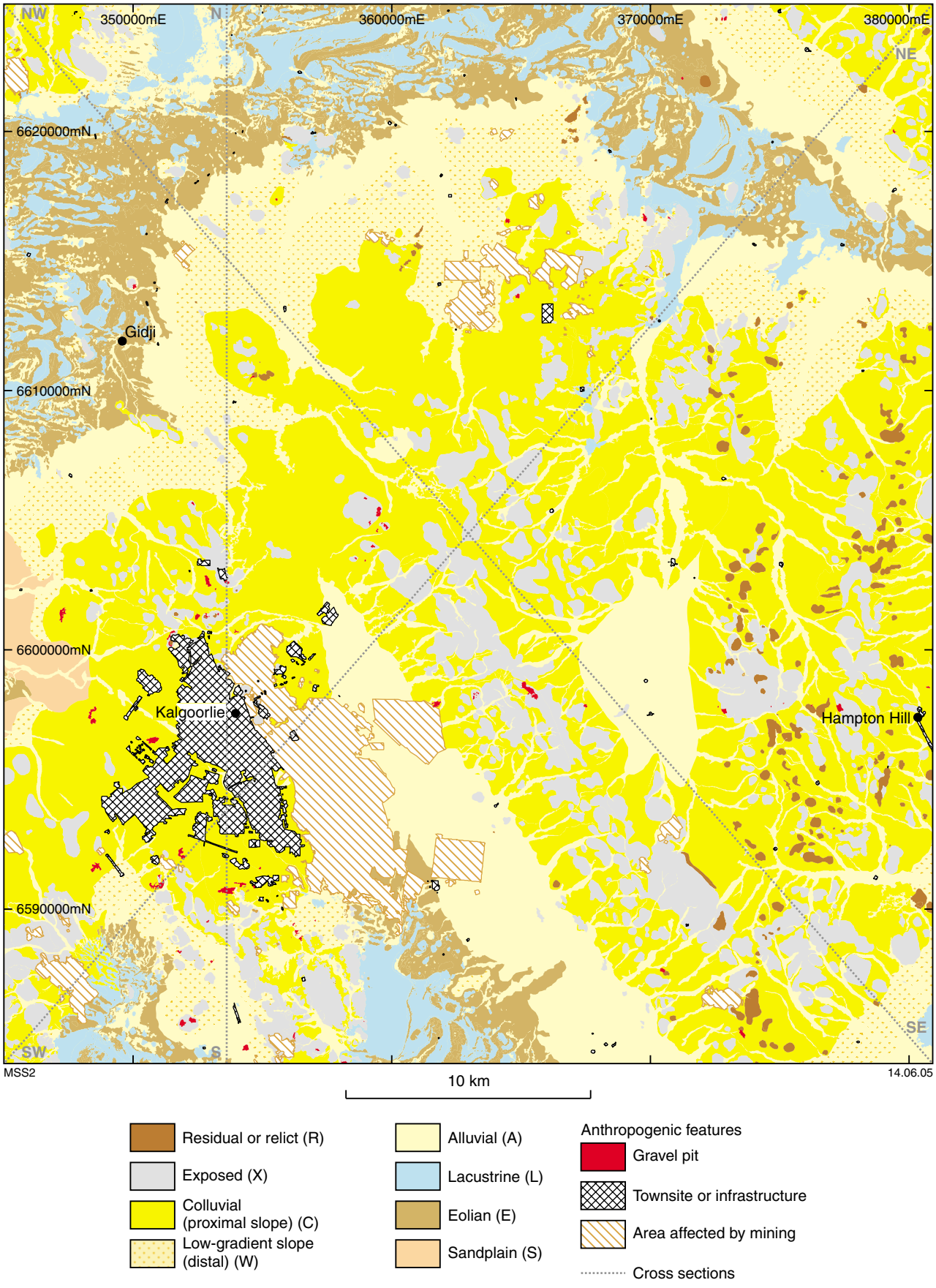

Figure 3. Distribution of regolith–landform units according to primary landform category

materials of the older pediment were derived from the weathering and erosion of the ranges and have blanketed pre-existing topographic relief. Thin (generally <2 m), more-recent alluvial and/or eolian cover may form a veneer over saprolite.

Ferruginous materials include ferruginized saprolite, which is found on hill crests and rises and overlying saprolite, as well as cemented polymictic ferruginous gravels that are found either along former drainage lines or as scree deposits (valley-fill) along hill slopes. The latter are found at various levels in the landscape. Material derived by weathering of cemented gravel on hills and ranges may form local pediments (unit $C_e f$). Elsewhere, skeletal soils (commonly calcareous), with lag derived locally, are common.

Eolian–playa domain

This domain corresponds to the Kunanalling, Black Flag, Hannan, and Yindarlgooda arms of the Roe Palaeochannel (Kern, 1995, 1996), an arcuate northeasterly to easterly zone to the north and northwest of Kalgoorlie, with smaller tributaries further south around Binduli. The main components are playas and playa margins, dunes, and eolian sandplains. Internal drainage is via linear depressions and swales. Low hills (with outcrop) locally occur on the western margins of some playas. Hematite-cemented coarse quartz sand is restricted to this domain and forms thin sheets that locally outcrop on playa shorelines. Silcrete is relatively common, particularly at or near the domain boundaries, or within palaeovalleys.

Distribution of regolith–landform units

The distribution of regolith–landform units is shown in Figure 4. Regolith–landform units are discussed in Appendix 3, on the basis of occurrence, topographic setting, regolith materials, and other information, such as Landsat signature. Except for quartz veins with surrounding rubble (*Xq*), units under the category X (low hills or rises with weathered or fresh lithologies) are not discussed; neither are anthropogenic units (e.g. gravel pits and quarries, areas affected by mining, and townsite or infrastructure areas).

Generalized distribution of regolith materials and their relationship to regolith–landform units

Three schematic topographic cross sections (Figs 5–7) outline the general distribution of regolith materials with respect to the regolith–landform units. Each section line represents the general distribution of regolith materials at or below the surface within a corridor 300 m wide. The sections were drawn using actual data from drillholes logged during field work, or from logs provided by Placer Dome Asia Pacific Inc. The locations of the schematic sections are shown on Figure 3.

Northwest–southeast cross section

This section (Fig. 5) extends from the northwestern corner of the map to the southeastern corner. It traverses pediment with outcrop in the northwest, through playas and eolian sandplain, the transitional zone to pediment, across the main pediment (including alluvial plain), and ends on the edge of alluvial plain in the southeast.

Pediments are characterized by thin, commonly calcareous, soils and outcrops of weathered bedrock. Shallow valleys are filled by ferruginous gravel (commonly cemented) and sheets or lenses of silcrete. Cementation of the gravel and erosion of surrounding regolith may give rise to topographic inversion, with cemented ferruginous gravel cappings on ridge and hill crests overlying saprolite and, less commonly, weakly weathered bedrock.

In the area designated playas and eolian sandplain, transported regolith infills valleys. Silcrete lenses lie within transported regolith at the margin of pediment. Subhorizontal marker horizons, such as coarse quartz sand cemented by hematite, appear in the transported regolith profile.

The saprolite–bedrock interface is irregular, with maximum thickness of saprolite approaching 80 m (Fig. 5).

Southwest–northeast cross section

This profile (Fig. 6) extends from the southwestern corner of the map to the northeastern, and transects pediment with narrow playas and eolian sandplain as well as alluvial plain, with a more substantial section of playas and eolian sandplain in the northeast. In the extreme southwest, the steplike land surface implies at least two peneplanation surfaces. To the northeast, narrow valleys between low hills are filled by transported material. In the far northeast, a broad shallow valley (eolian–playa domain) is filled by transported clays, and includes a cemented ferruginous gravel horizon.

North–south cross section

This section (Fig. 7) transects a major portion of playas and eolian sandplain, together with transitional zone to pediment, pediment, and alluvial plain in the south. In the area of playas and eolian sandplain the thickness of transported regolith varies considerably between 8 and 34 m. Thin, horizontal marker horizons lie at shallow

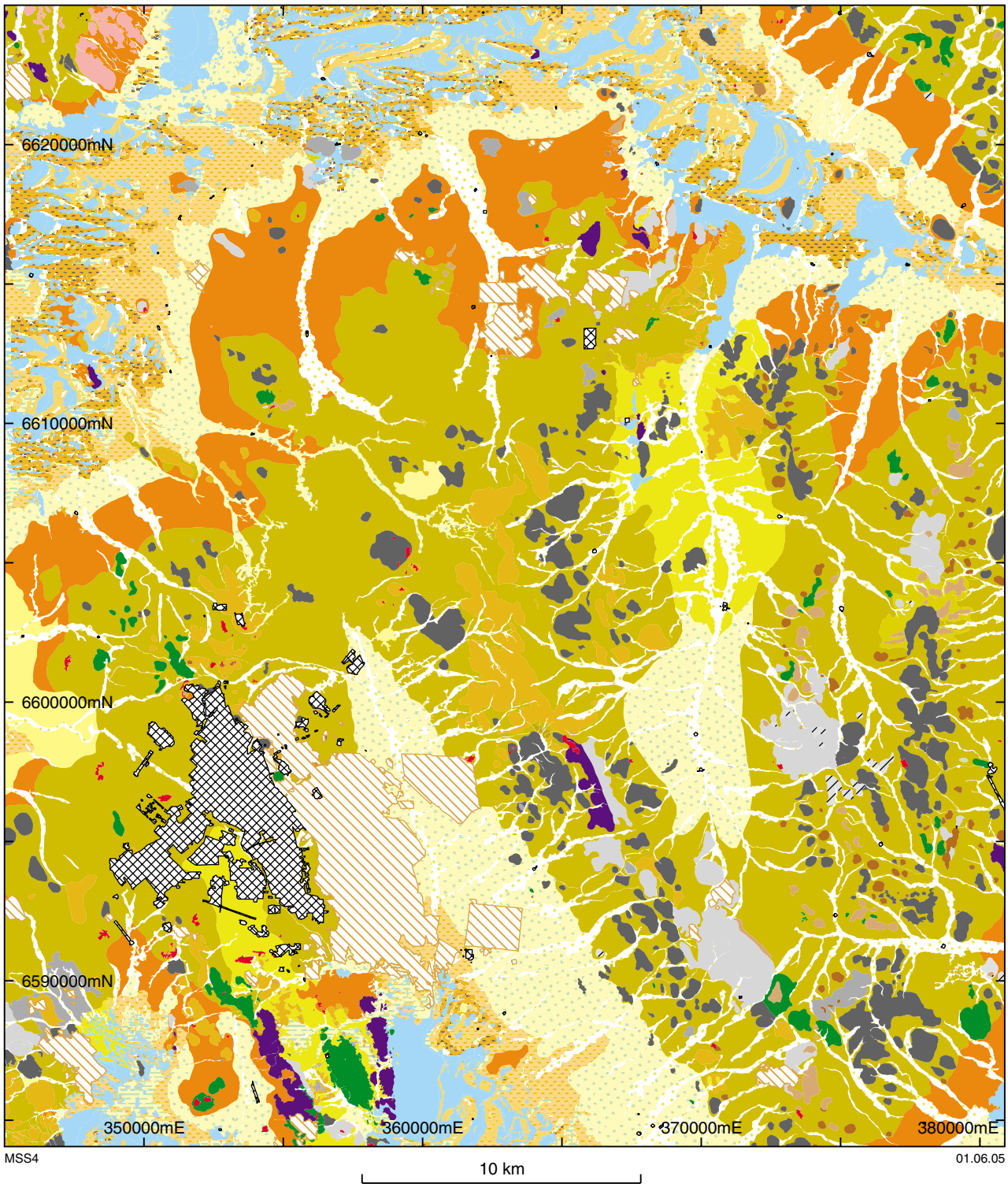

Figure 4. Simplified regolith–landform map of the Kalgoorlie–Kanowna area showing distribution of regolith–landform units. This diagram has been compiled from the database, and many small regolith occurrences may not be easily visible at this scale

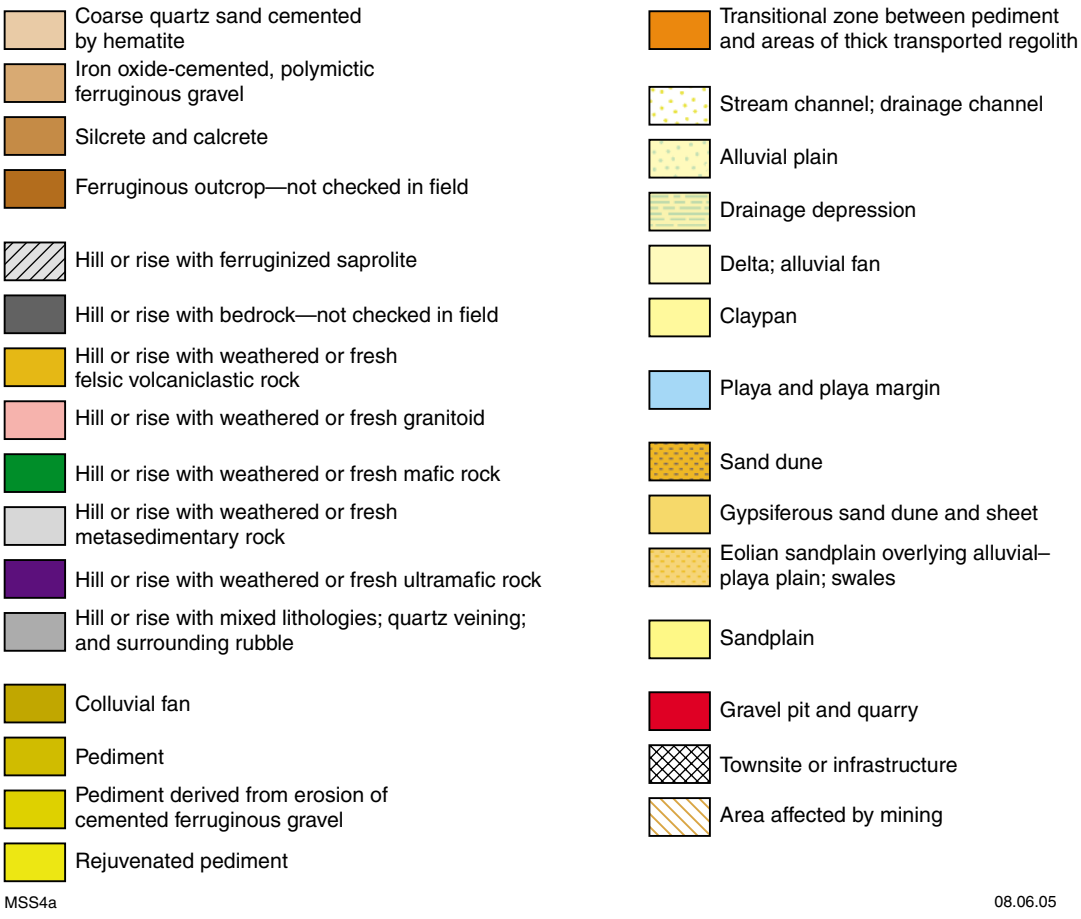
Coarse quartz sand cemented by hematite
Iron oxide-cemented, polymictic ferruginous gravel
Silcrete and calcrete
Ferruginous outcrop—not checked in field
Hill or rise with ferruginized saprolite
Hill or rise with bedrock—not checked in field
Hill or rise with weathered or fresh felsic volcaniclastic rock
Hill or rise with weathered or fresh granitoid
Hill or rise with weathered or fresh mafic rock
Hill or rise with weathered or fresh metasedimentary rock
Hill or rise with weathered or fresh ultramafic rock
Hill or rise with mixed lithologies; quartz veining; and surrounding rubble
Colluvial fan
Pediment
Pediment derived from erosion of cemented ferruginous gravel
Rejuvenated pediment
Transitional zone between pediment and areas of thick transported regolith
Stream channel; drainage channel
Alluvial plain
Drainage depression
Delta; alluvial fan
Claypan
Playa and playa margin
Sand dune
Gypsiferous sand dune and sheet
Eolian sandplain overlying alluvial–playa plain; swales
Sandplain
Gravel pit and quarry
Townsite or infrastructure
Area affected by mining
MSS4a
08.06.05

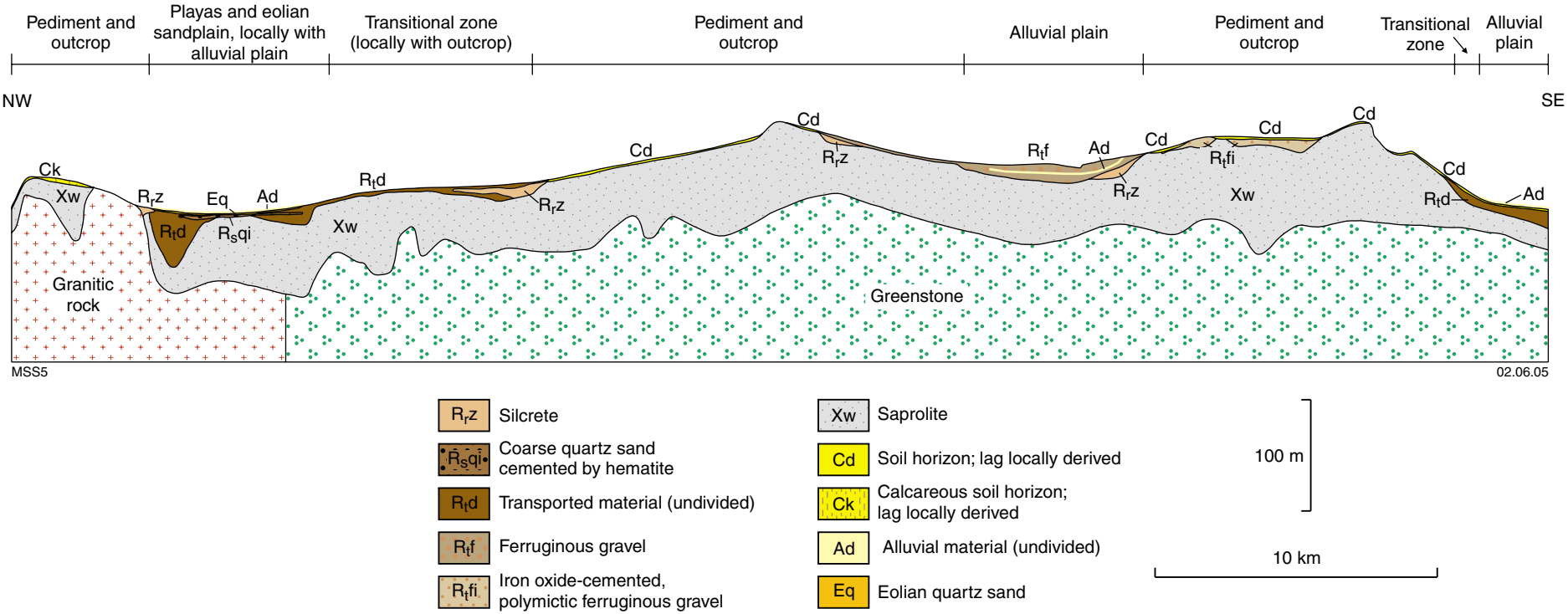

Figure 5. Schematic cross section showing regolith materials (according to regolith–landform unit), from the northwestern corner of the map to the southeastern corner (see Figure 3 for location)

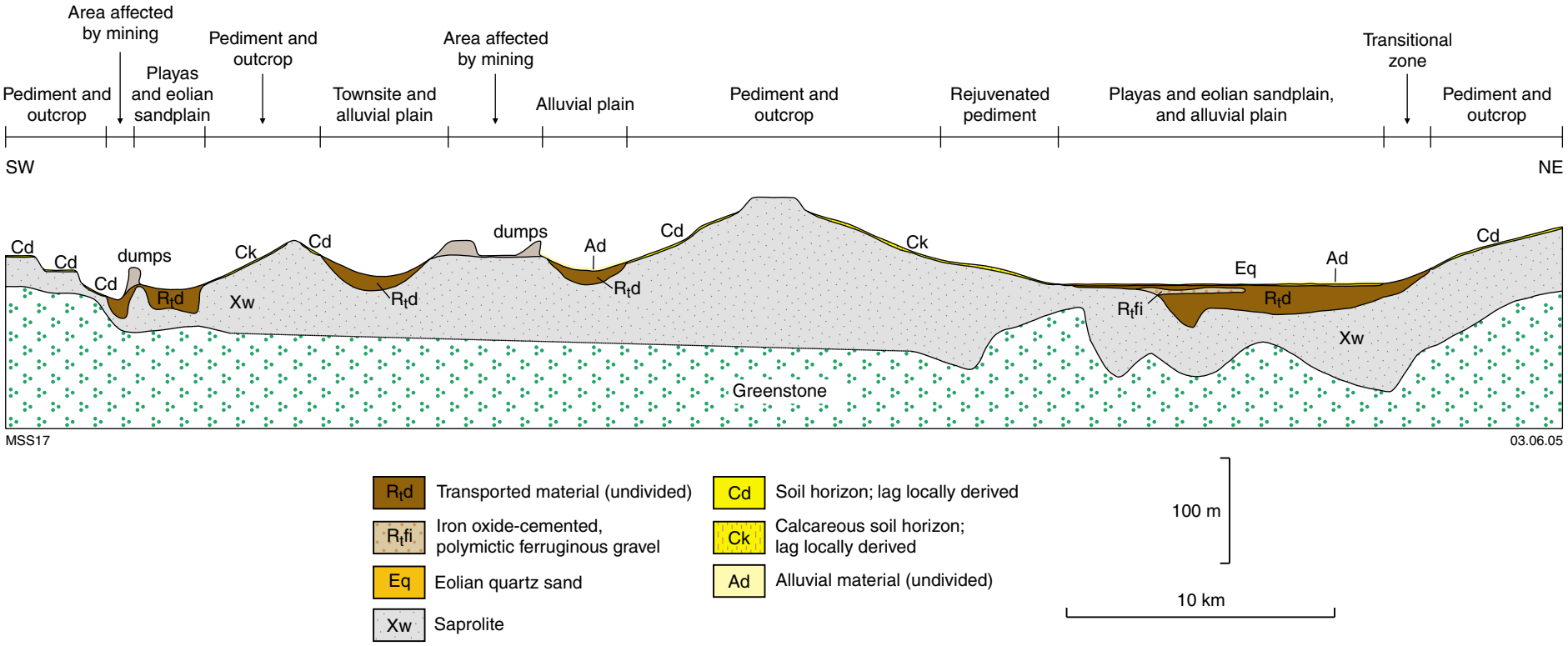

Figure 6. Schematic cross section showing regolith materials (according to regolith–landform unit), from the southwestern corner of the map to the northeastern corner (see Figure 3 for location)

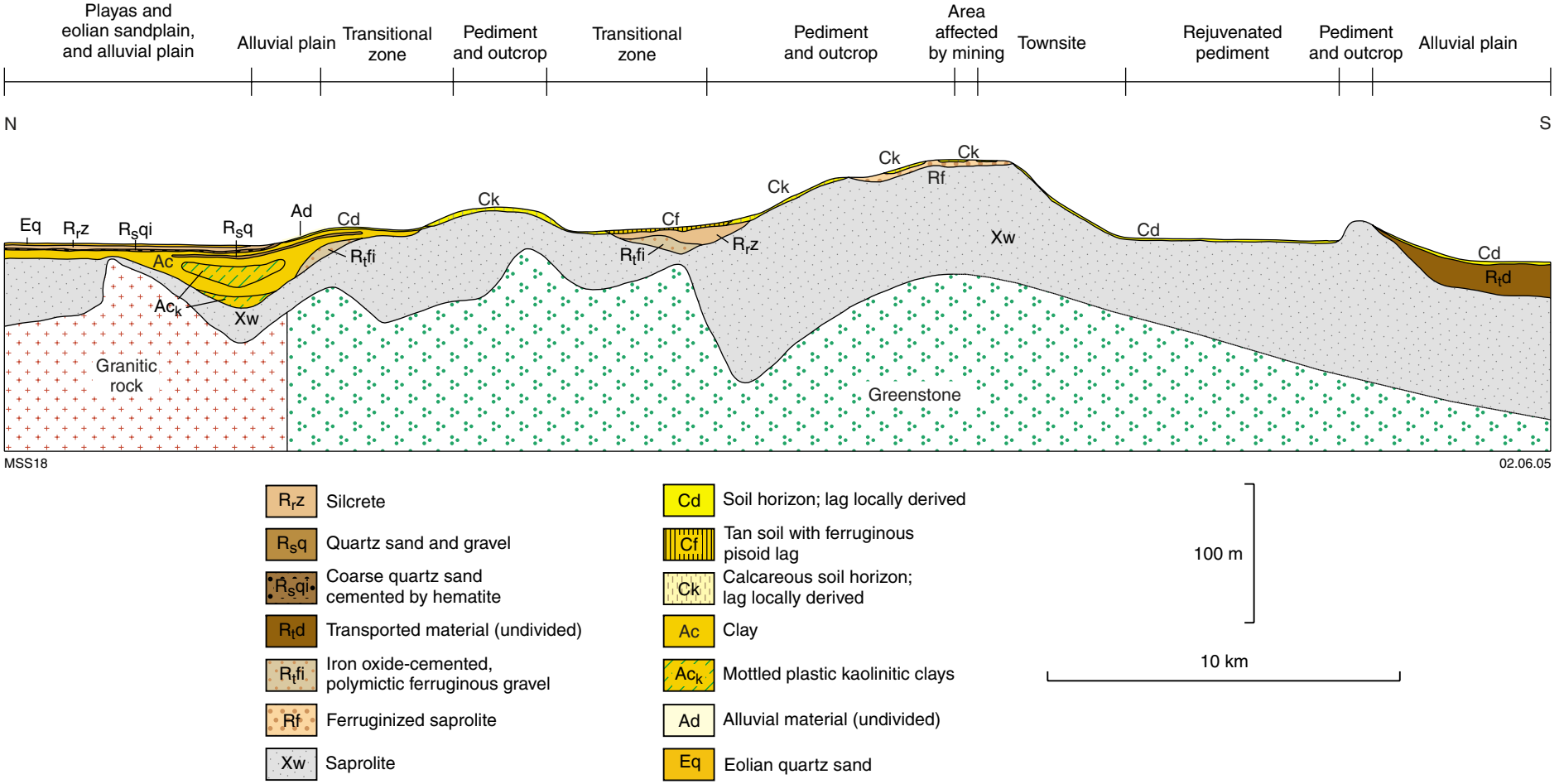

Figure 7. Schematic cross section showing regolith materials (according to regolith–landform unit), from north to south in the vicinity of grid line 353600E (see Figure 3 for location)

depth beneath a veneer of eolian sand. These are: silcrete overlying coarse quartz sand cemented by hematite, clays, and quartz sand and gravel. Some of these units extend into the transported regolith of the transitional zone. Lenses of ferruginous gravel may be present along valley sides and mottled plastic clays lie in deeper parts of infilled palaeovalleys.

Shallow valleys at the margins of pediment are filled by cemented ferruginous gravel overlain by silcrete sheets. Tan soils have significant ferruginous pisoid lag.

On low hills and rises on pediment, thin, skeletal calcareous soils overlie ferruginous saprolite or ferruginized saprolite, above a considerable thickness of saprolite (up to 80 m). In the south, a planation surface (rejuvenated pediment) has been cut into this older peneplain. The saprolite–bedrock interface is irregular, with local basement highs beneath transported regolith in the north.

Conclusions

Regolith–landforms in the Kalgoorlie–Kanowna area occur in two principal domains:

a) a colluvial–relict domain — characterized by low hills and rises (commonly with outcrops of variably weathered bedrock), surrounded by a broad pediment and fringed by a transitional zone, exhibiting underlying pediment structure but overlain by up to 25 m of transported material; and

b) the eolian–playa domain — comprising superficial eolian and playa deposits overlying alluvial material of a relict fluvial system.

Regolith–landform mapping, together with field observations, demonstrates that there is a close association between the geological framework and landforms that can be used to derive an interpretation of near-surface regolith. Pediment and hills outline areas of outcrop, colluvium, and thin transported cover. The topographic contour patterns of the colluvial–relict domain disappear where cover is significantly thicker in the eolian–playa domain.

From a mineral exploration perspective, regolith–landform maps enable a clear indication of which geochemical sampling techniques can be applied to specific areas. In colluvial–relict domains, soil, lag, rock-chip sampling, and shallow drilling are likely to be effective techniques, whereas in eolian–playa domains surface geochemical sampling methods are less likely to succeed and deeper drilling may be required. In addition, characterization of regolith materials is important, in that it can influence sampling media. For example, cemented (and transported) ferruginous gravel on hill crests has not developed from the underlying saprolite and, consequently, the geochemical response from the gravel is not related to that of the underlying saprolite.

Acknowledgements

Placer Dome Asia Pacific Inc. facilitated access to lithological data from their drilling database.

The airborne hyperspectral survey was a collaborative project with the Commonwealth Scientific and Industrial Research Organisation (CSIRO), HyVista Corporation, Cooperative Research Centre for Landscape Evolution and Mineral Exploration (CRC LEME), Placer Dome Asia Pacific Inc., and the Minerals and Energy Research Institute of Western Australia (MERIWA).

References

ANAND, R. R., CHURCHWARD, H. M., SMITH, R. E., SMITH, K., GOZZARD, J. R., CRAIG, M. A., and MUNDAY, T. J., 1993, Classification and atlas of regolith–landform mapping units, Exploration perspectives for the Yilgarn Craton: Australia, CSIRO Division of Exploration and Mining, Restricted Report 440R (unpublished).

CHAN, R. A., CRAIG, M. A., HAZELL, M. S., and OLLIER, C. D., 1992, Kalgoorlie regolith terrain map commentary, Sheet SH51 Western Australia, 1:1 000 000 Regolith Series: Australia, Bureau of Mineral Resources, Geology and Geophysics (now Geoscience Australia), Record 1992/8, 71p.

CHAN, R. A., OLLIER, C. D., and GIBSON, D. L., 1988, Regolith terrain data — Kalgoorlie 1:1 000 000 sheet SH51, Western Australia: Australia, Bureau of Mineral Resources, Geology and Geophysics, Record 1988/3, 74p.

CRAIG, M. A., and ANAND, R. R., 1993, Kalgoorlie–Kurnalpi regolith–landforms 1:250 000 special edition map: Australian Geological Survey Organisation and Cooperative Research Centre for Australian Mineral Exploration Technologies.

CUDAHY, T., CACCETTA, M., CORNELIUS, A., HEWSON, R., WELLS, M., SKWARNECKI, M., and HAUSKNECHT, P., 2005a, Kalgoorlie–Kanowna kaolin disorder, part sheets 3136 and 3236: Geological Survey of Western Australia 1:100 000 map.

CUDAHY, T., CACCETTA, M., CORNELIUS, M., HEWSON, R., WELLS, M., SKWARNECKI, M., HALLEY, S., and HAUSKNECHT, P., 2005b, Hyperspectral regolith and alteration mineral mapping of the Kalgoorlie–Kanowna 1:100 000 scale mapsheet: Perth, Cooperative Research Centre for Landscape Environments and Mineral Exploration and Geological Survey of Western Australia, Minerals Seminar, Kalgoorlie, WA, 15–16 February, 2005, Abstracts, p. 24–28.

DELL, M. R., 1992, Regolith–landform relationships and geochemical dispersion about the Kanowna Belle Au deposit, W.A.: Hobart, University of Tasmania, BSc (Hons) thesis (unpublished).

EGGLETON, R. A. (editor), 2001, The regolith glossary — surficial geology, soils and landscapes: Perth, Cooperative Research Centre for Landscape Evolution and Mineral Exploration, 144p.

GEOLOGICAL SURVEY OF WESTERN AUSTRALIA, 2004, Regolith–landform resources of the Kalgoorlie–Kanowna region, 1:50 000: Western Australia Geological Survey, Record 2004/12, DVD.

GOZZARD, J. R., 2004, Predictive regolith–landform mapping: SEG2004 Predictive mineral discovery under cover, Workshop 1, How to look at, in and through the regolith for efficient predictive mineral discoveries, Workshop Notes: Part 2, 163p.

HOCKING, R. M., LANGFORD, R. L., THORNE, A. M., SANDERS, A. J., MORRIS, P. A., STRONG, C. A., and GOZZARD, J. R., 2001, A classification system for regolith in Western Australia: Western Australia Geological Survey, Record 2001/4, 21p.

KERN, A. M., 1995, Hydrogeology of the Kalgoorlie 1:250 000 sheet: Western Australia Geological Survey, 1:250 000 Hydrogeological Series Explanatory Notes, 16p.

KERN, A. M., 1996, Hydrogeology of the Kurnalpi 1:250 000 sheet: Western Australia Geological Survey, 1:250 000 Hydrogeological Series Explanatory Notes, 16p.

KRIEWALDT, M. J. B., 1969, Kalgoorlie W.A. (1st edition): Western Australia Geological Survey, 1:250 000 Geological Series Explanatory Notes, 17p.

KRIEWALDT, M., 1974, Quaternary geology, Kalgoorlie, Australia, with an addendum: The stratigraphic relationships of carbonate and gypsiferous deposits in the Kalgoorlie area: Perth, University of Western Australia, MSc thesis (unpublished).

LADHAMS, B. A., 1994, The sediments and regolith of the middle reaches of the Roe Palaeochannel near Kanowna, Eastern Goldfields, Western Australia: Perth, Western Australia, Curtin University of Technology, BSc (Hons) thesis (unpublished).

OLLIER, C. D., CHAN, R. A., CRAIG, M. A., and GIBSON, D. L., 1988, Aspects of landscape history and regolith in the Kalgoorlie region, Western Australia: Australia, BMR Journal of Australian Geology and Geophysics, v. 10, no. 4, p. 309–321.

PAIN, C., CHAN, R., CRAIG, M., HAZELL, M., KAMPRAD, J., and WILFORD, J., 1991, RTMAP, BMR Regolith database field handbook: Australia, Bureau of Mineral Resources, Geology and Geophysics, Record 1991/29, 125p.

RIGANTI, A., GROENEWALD, P. B., and McCABE, M., 2003, East Yilgarn Geoscience Database — a 100 000 reinterpretation of the Eastern Goldfields regolith: Western Australia Geological Survey, Record 2003/11, 21p.

TAPLEY, I. J., and GOZZARD, J. R., 1992, Regolith–landform mapping in the Lawlers District. Report 1: Aerial photographic interpretation and Landsat Thematic Mapper processing for mapping regolith–landforms: Perth, CSIRO and Institute of Minerals, Energy and Construction, Division of Exploration Geoscience, Restricted Report 239R, 131p.

Appendix 1

HyMap™ metadata (data provided by CSIRO, Perth June, 2005)

Additional Metadata

Product Name	Estimated Abundance/Chemistry	Product Description	Accuracy Assessment
albedo	N/A	Similar to B&W aerial photograph. Radiance at 1000 nm.	N/A
Amphibole abundance	15% (blue) to 50% (red) relative abundance*. Linear. 	Continuum-removed depth of the amphibole (actinolite-tremolite) absorption centred at 2330 nm and masked for: (1) ferrous iron absorption (included); (2) surface water (excluded); and (3) low albedo @1000nm (excluded).	**low**. Potential spectral mixing with talc, especially in areas of oxidation, i.e. iron oxide development.
chlorite abundance	15% (blue) to 50% (red) relative abundance*. Linear. 	Continuum-removed depth of the chlorite absorption centred at 2250 nm and masked for: (1) ferrous iron absorption (included); (2) surface water (excluded); and (3) low albedo @1000nm (excluded).	**moderate**. Abundance based only two HyMap bands within the narrow diagnostic chlorite absorption feature.
chlorite chemistry	Chlorite Mg number [MgO/(MgO+FeO)]; #1 (purple: Mg-rich) to #0 (Red: Fe-rich). Histogram equalise. 	Continuum-removed wavelength position of the chlorite absorption centred at 2250 nm and masked for : (1) ferrous iron absorption (included); (2) surface water (excluded); and (3) low albedo @1000nm (excluded).	**low**. Wavelength determination is based on only two HyMap bands within as well bands on the shoulders of the diagnostic chlorite absorption feature.
dry vegetation abundance	25% (blue) to 100% (red) relative abundance. Linear. 	Continuum-removed depth of the cellulose absorption band near 2100 nm. Masked for low albedo @1000nm (excluded).	**moderate**. Potential confusion with pixels containing serpentine (also has a feature near 2100 nm) and surface water. Note anomalously high dry vegetative cover associated with large ultramafic bodies near Kanowna and Mount Hunt.
Gypsum abundance	Blue (25%) to Red (100%) relative abundance*. Linear. 	Continuum-removed depth of the gypsum absorption centred at 1535 nm and masked for: (1) presence of 1750 nm absorption (inclusive); and (2) low albedo @1000nm (excluded).	**high**. Note though the HyMap spectra show the diagnostic gypsum absorptions are double the depth of the USGS library spectra. There is also Isolated noise associated with vegetation.

Hematite-goethite ratio for iron oxide rich regolith	Hematite-Goethite ratio (H/G) for pixels with 25–30% iron oxide relative abundance* only. Red (H/G: 1) to Yellow (H/G: 0). Linear. 	Continuum-removed wavelength of the 900 nm ferric oxide absorption and masked for: (1) iron oxide abundance above 25% (included); and (2) low albedo @1000nm (excluded).	**moderate.** Difficulties in scene-dependent reduction to reflectance (largely atmospheric effects) have caused problems establishing the background slope (continuum) for pixel spectrum necessary for measuring the wavelength position. This has resulted in poor seamless products.
hematite-goethite ratio all iron oxides	Hematite-Goethite ratio (H/G) for pixels with 5–30% iron oxide relative abundance*. Red (H/G: 1) to Yellow (H/G: 0). Linear. 	Continuum-removed wavelength of the 900 nm ferric oxide absorption and masked for: (1) iron oxide abundance above 25% (included); and (2) low albedo @1000nm (excluded).	**moderate.** Difficulties in scene-dependent reduction to reflectance (largely atmospheric effects) have caused problems establishing the background slope (continuum) for pixel spectrum necessary for measuring the wavelength position. This has resulted in poor seamless products.
iron oxide abundance	5% (blue) to 30% (red) relative abundance*. Linear. 	Continuum-removed depth of the ferric oxide (hematite-goethite) absorption centred at 900 nm and masked for low albedo @1000nm (excluded).	**high.** Based on XRF versus field/airborne measurements, error estimate is +/- 10% Fe_2O_3.
kaolin abundance	15% (blue) to 80% (red) relative abundance*. 	Continuum-removed depth of the kaolin absorption (kaolinite, dickite, halloysite) centred at 2206 nm and masked for: (1) 2350 nm absorption (excluded); (2) kaolin absorption at 2160 nm (included); and (3) low albedo @1000nm (excluded).	**high.** Based on LOI/XRD versus field/airborne measurements, error estimate is +/- 15% kaolin abundance.
kaolin disorder	Poorly-ordered (blue) to well-ordered (red). 	Continuum-removed depth of the kaolin absorption (kaolinite, dickite, halloysite) centred at 2160 nm and masked for: (1) for kaolin abundance; and (2) low albedo @1000nm (excluded).	**high.** Based on XRD versus field/airborne statistical assessment, this parameter is sensitive to the kaolinite c-basal spacing (001 hkl XRD reflection).
pyrophyllite abundance	Blue (20%) to Red (40%) relative abundance*. 	Continuum-removed depth of the pyrophyllite absorption centred at 2175 nm and masked for: (1) the 2320 nm absorption (included); (2) the gypsum 1550 nm feature (excluded); (3) the Al-OH absorption at 2200 nm (excluded); and (4) low albedo @1000nm (excluded).	**high**. HyMap derived pyrophyllite areas not yet sampled. Identification based on spectral matching with USGS library mineral spectra only.

surface water abundance	Low (blue) to high (red) abundances of water found at the surface in green vegetation and various minerals. No quantitative estimates determined. 	Continuum-removed depth of the surface water absorption centred at 1180 nm and not masked.	**moderate**. This water absorption can be found in a variety of surface materials (not atmospheric water vapour) and is non-specific in its origin. That is, can be developed in green vegetation (most common), standing water and water associated with minerals like illite, kaolin (e.g. halloysite), and smectite.
talc abundance	10% (blue) to 35%(red) relative abundance*. 	Continuum-removed depth of the talc/amphibole absorption centred at 2314 nm and masked for: (1) ferrous iron (excluded to separate actinolite from talc); (2) surface water (excluded); and (3) low albedo at 1000 nm (excluded).	**moderate**. The separation of talc from amphibole is essentially based on the amount of ferrous iron, which can be complicated by iron oxides as well as the development of tremolite rather than actinolite/hornblende. Vegetation can also complicate/absorb at 2314 nm.
water associated with all iron oxides	Low (blue) to high (red) abundances. No quantitative estimates determined. 	Continuum-removed depth of the surface water absorption centred at 1180 nm and masked for: (1) iron oxide abundance; and (2) low albedo at 1000 nm (excluded).	**moderate.** This water can be associated with any of a variety of mineral found within a given pixel, including, iron oxide, kaolin, illite, and smectite.
water associated with iron oxide rich regolith	Low (blue) to high (red) abundances. No quantitative estimates determined. 	Continuum-removed depth of the surface water absorption centred at 1180 nm and masked for: (1) iron oxide abundance; and (2) low albedo at 1000 nm (excluded).	**moderate.** This water can be associated with any mineral within given pixel, including, iron oxide, kaolin, illite, and smectite.
water associated with white mica	Low (blue) to high (red) abundances. No quantitative estimates determined. 	Continuum-removed depth of the surface water absorption centred at 1180 nm and masked for: (1) white mica abundance and; (2) low albedo @1000nm (excluded).	**moderate.** This water can be associated with any mineral within given pixel, including, iron oxide, kaolin, illite, and smectite. High water contents in white mica possibly associated with illite/brammallite.
water associated with kaolin	Low (blue) to high (red) abundances. No quantitative estimates determined. 	Continuum-removed depth of the surface water absorption centred at 1180 nm and masked for: (1) kaolinite abundance and; (2) low albedo @1000nm (excluded).	**moderate.** This water can be associated with any mineral within given pixel, including, iron oxide, kaolin, illite, and smectite.

white mica abundance (kaolin filtered)	25% (blue) to 90% (red) relative abundance*. 	Continuum-removed depth of the white mica absorption centred at 2200 nm and masked for: (1) presence of 2350 nm absorption; (2) kaolin absorption at 2160 nm and; (3) low albedo @1000nm (excluded).	**high to moderate.** Pixels containing white mica and kaolin have been masked out so there are omission inaccuracies, though for those pixels without kaolin, the accuracy of the white mica estimates are high.
white mica abundance (no kaolin filter)	~10% (purple) to 25% (blue) to 90% (red) relative abundance*. 	Continuum-removed depth of the white mica absorption centred at 2200 nm and masked for (1) presence of 2350 nm absorption; and; (2) low albedo @1000nm (excluded).	**moderate to low.** The estimates for the abundance levels for white mica are poorer because of possible mixing effects with kaolin.
white mica chemistry (kaolin filter)	Wavelength position from 2180 nm (blue), which equates to 4.0 mica $R^{III}_{(oct)}$ to 2215 nm, which equates to 3.2 mica $R^{III}_{(oct)}$ in the level Tschermak^{+} substitution for only those pixels that contain white mica and no kaolin. 	Continuum-removed wavelength of the white mica absorption centred at 2200 nm and masked for: (1) presence of 2350 nm absorption (included); (2) Al-OH absorption at 2200 nm (included); (3) kaolin absorption at 2160 nm (excluded) and; (4) low albedo @1000nm (excluded).	**high.** Pixels containing white mica and kaolin have been masked out so there are omission inaccuracies, though for those pixels without kaolin, the accuracy of the white mica estimates are high.
white mica chemistry (no kaolin filter) • *linear* • *non-linear*	Wavelength position from 2180 nm (blue), which equates to 4.0 mica $R^{III}_{(oct)}$ to 2215 nm, which equates to 3.2 mica $R^{III}_{(oct)}$ in the levels Tschermak substitution^{+} for all pixels that contain white mica ± kaolin. 	Continuum-removed wavelength of the white mica absorption centred at 2200 nm and masked for: (1) presence of 2350 nm absorption (included); (2) Al-OH absorption at 2200 nm (included); and; (3) low albedo @1000nm (excluded). Pseudo colour stretched using: • Linear; and • Histogram equalisation.	**moderate.** Pixels containing white mica and kaolin have been included such that the wavelength is a function of both and not white mica alone, though for those pixels without kaolin, the accuracy of the white mica estimates are high.

* No proportional abundance correction for the mineral of interest in rock/soil mixed with vegetation at the pixel level

+ $[(\text{vacancy/Mg/Fe}^{2+}_{(oct)} + \text{Si}_{(tet)}) \Leftrightarrow (\text{Al}_{(oct)} + \text{Al}_{(tet)})]$.

Appendix 2

Regolith codes: on maps and in the database

New map code	*New database code*
R_rk	_Rr-k
R_rz	_Rr-z
$R_s$qi	_Rs-q-i
$R_t$fi	_Rt-f-i
Rf	_R-f
X_ld	_Xl-d
X_ld$_w$	_Xl-dw
X_ld$_w$i	_Xl-dw-i
X_ll	_Xl-l
$X_l$ds	_Xl-d-s
X_ld$_w$s	_Xl-dw-s
X_lg$_w$	_Xl-gw
$X_l$gp	_Xl-g-p
$X_l$gv	_Xl-g-v
X_lm	_Xl-m
X_lm$_w$	_Xl-mw
X_lu	_Xl-u
X_lu$_w$	_Xl-uw
Xq	_X-q
C$_a$	_Ca
C$_e$	_Ce
C$_e$f	_Ce-f
C$_j$	_Cj
W$_e$	_We
A$_a$	_Aa
A$_c$	_Ac
A$_d$	_Ad
A$_e$	_Ae
A$_p$c	_Ap-c
A$_u$	_Au
A$_v$	_Av
A$_y$	_Ay
L$_m$	_Lm
L$_p$	_Lp
E$_e$	_Ee
E$_e$e$_g$	_Ee-eg
E$_p$e$_g$	_Ep-eg
E$_s$	_Es
E$_w$	_Ew
S	_S

Appendix 3

Descriptions of regolith–landform map units (listed by primary landform unit)

Appendix 3

Residual or relict (R)

R_rk Calcrete — Figures 3.1–3.2

Occurrence: in soil profiles in colluvial–relict domain; appears to be absent from the eolian–playa domain.

Topographic setting: calcareous soils with nodular calcrete on low hills and rises and sandplain; on alluvial plains or along rejuvenated pediment margins.

Regolith materials: vary from powdery calcrete in soils, to nodular and massive horizons in soil profiles.

Database code: _Rr-k

MSS15 30.05.05

Figure 3.1. Close-up of nodular calcrete (*R*$_r$*k*) overlying cemented ferruginous gravel. Sample site 255777 (343755E 6622685N)

MSS64 30.05.05

Figure 3.2. Nodular calcrete (*R*$_r$*k*) below thin soil horizon (0.15 m thick) on sandplain. Sample site 256930 (348570E 6597140N)

Residual or relict (R) (cont.)

R_rz Silcrete — Figures 3.3–3.5

Occurrence: in transported regolith and at contacts between colluvial–relict and transported regolith at the margins of valley-fill sediments.

Topographic setting: at low points, at playa margins, and in transported regolith profiles.

Regolith materials: silcrete; commonly megamottled; also chalcedonic veining; developed from saprolite over greenstones and granitic rocks at colluvial–relict domain boundaries, or by precipitation–cementation from silica-bearing groundwaters in transported regolith in shallow valleys.

Database code: _Rr-z

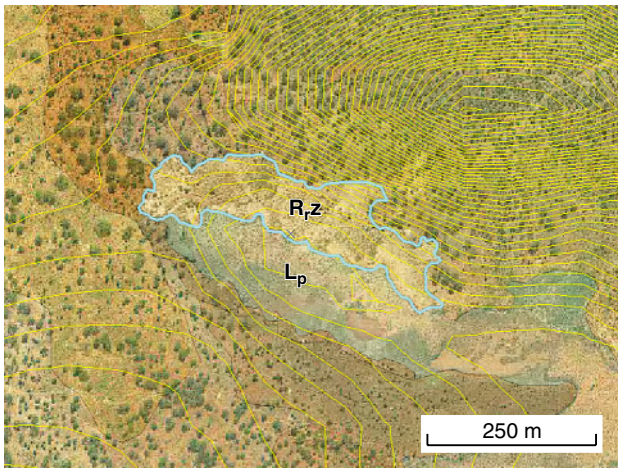

MSS61 30.05.05

Figure 3.3. Silcrete — orthophotographic image overlain by silcrete polygon (R_rz) at edge of playa (L_p). The central point of the image is 356000E 6619785N

MSS62 30.05.05

Figure 3.4. Megamottled silcrete on playa shoreline. The silcrete is overlain by calcareous soil and massive calcrete (in background). Sample site 255862 (356145E 6619740N)

MSS63 30.05.05

Figure 3.5. Close-up of megamottling in silcrete. Sample site 255862; length of the pen is 13.5 cm

Residual or relict (R) (cont.)

$R_s$qi Coarse quartz sand cemented by hematite — Figures 3.6–3.7

Occurrence: most commonly as outcrop or subcrop along playa shorelines; forms a continuous marker horizon 1–3 m thick (where intersected by drilling) at shallow depth (1–5 m) in the transported regolith profile.

Topographic setting: at low points of the topography, along playa shorelines.

Regolith material: coarse quartz sand and rare pebbles cemented by hematite.

Database code: _Rs-q-i

MSS13 30.05.05

Figure 3.6. Subcrop of unit of coarse quartz sand cemented by (*$R_s$qi*) hematite along playa shoreline. Sample site 255820, looking southwest (347425E 6614685N)

MSS54 30.05.05

Figure 3.7. Close-up of subcrop of coarse quartz sand cemented by hematite (*$R_s$qi*). Sample site 255820; length of pen is 13.5 cm

Residual or relict (R) (cont.)

$R_t$fi Iron oxide-cemented, polymictic ferruginous gravel Figures 3.8–3.14

Occurrence: in both colluvial–relict and eolian–playa domains; typically as steep-sided, flat-topped ridges.

Topographic setting: hill and ridge crests; originally formed as valley-fill along drainages; now occupying crests of hills and rises, which indicates topographic inversion; in the subsurface, as valley-fill (from drillhole logs).

Regolith materials: cemented polymictic gravel, comprising pebbles of ferricrete, ferruginous saprolite, quartz and maghemitic pisoids, matrix- to clast-supported, with a goethite–clay matrix; some varieties have goethitic cutans around clasts; hematitic (indurated) on ridge crests, but goethitic farther down the topographic or weathering profile.

Database code: _Rt-f-i

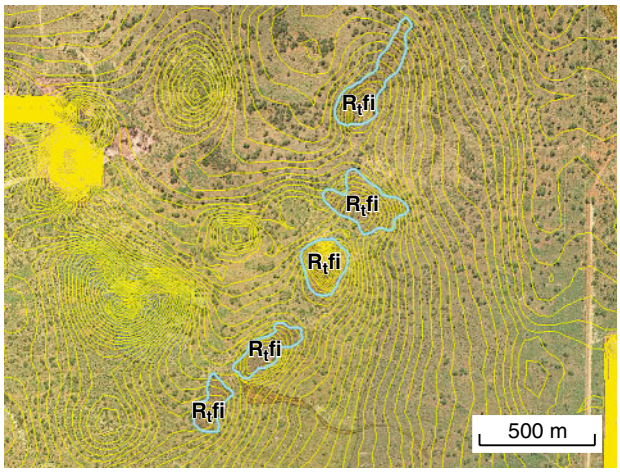

MSS55 30.05.05

Figure 3.8. Iron oxide-cemented, polymictic ferruginous gravel — orthophotographic image overlain by cemented ferruginous gravel polygons (*$R_t$fi*) along low hills and ridges across the contact between pediment and the transitional zone. The central point of the image is 360935E 6615440N

MSS56 30.05.05

Figure 3.9. Outcrop of indurated iron oxide-cemented, ferruginous gravel along low ridge. Sample site 255977 (373990E 6592395N)

MSS57 30.05.05

Figure 3.10. Close-up of outcrop of indurated iron oxide-cemented, ferruginous gravel showing cemented ferruginous clasts. Sample site 255977; length of pen is 13.5 cm

$R_t$fi Iron oxide-cemented, polymictic ferruginous gravel (cont.)

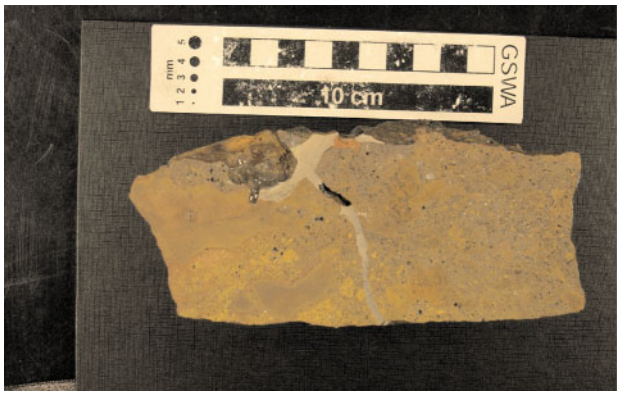

MSS58 30.05.05

Figure 3.11. Cemented ferruginous gravel comprising dominantly locally derived clasts of ferruginous saprolite, and minor rounded quartz. It may be indicative of a relatively short distance of transport. Sample site MSS3355 (372400E 6590030N). The apparent veining is epoxy resin glue

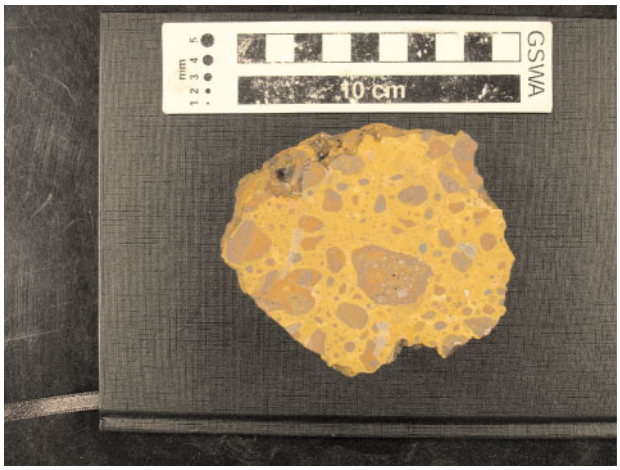

MSS14 18.04.05

Figure 3.12. Matrix-supported (goethitic clays), cemented polymictic ferruginous gravel. The clasts comprise quartz, ferruginous saprolite, ferricrete, and maghemitic pisoid lag. Sample site 256145 (373145E 6603315N)

MSS59 30.05.05

Figure 3.13. Matrix-supported, polymictic ferruginous gravel. Clasts are dominantly maghemitic pisoid lag with minor ferruginous saprolite. Sample site 256020 (375445E 6592205N)

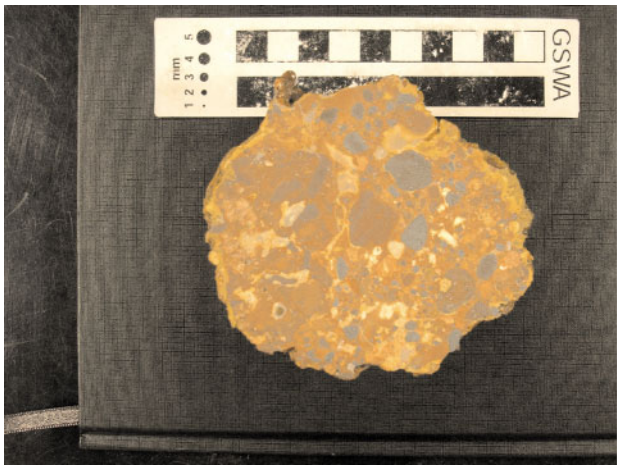

MSS60 30.05.05

Figure 3.14. Clast-supported, cemented polymictic ferruginous gravel. The clasts comprise ferruginous saprolite, saprolite, maghemitic pisoid lag, ferricrete, and quartz. Some of the clasts appear to have been reworked. Sample site 256138 (374250E 6599940N)

Residual or relict (R) (cont.)

Rf Ferruginous material — not checked in the field

Occurrence: generally in the colluvial–relict domain; spatially related to iron oxide-cemented polymictic ferruginous gravel, ferruginized saprolite outcrops, and ferruginous duricrust.

Topographic setting: on low rises and hill crests.

Regolith materials: ferruginous.

Database code: _R-f

Exposed (X)

$X_l d_w i$ Ferruginized saprolite — Figures 3.15–3.18

Occurrence: dominantly indurated (ferruginized and silicified) saprolite and ferruginous saprolite; may be spatially related to iron oxide-cemented polymictic ferruginous gravel.

Topographic setting: on low rises and hill crests.

Regolith materials: massive, fine-grained, siliceous and/or ferruginous materials.

Database code: _Xl-dw-i

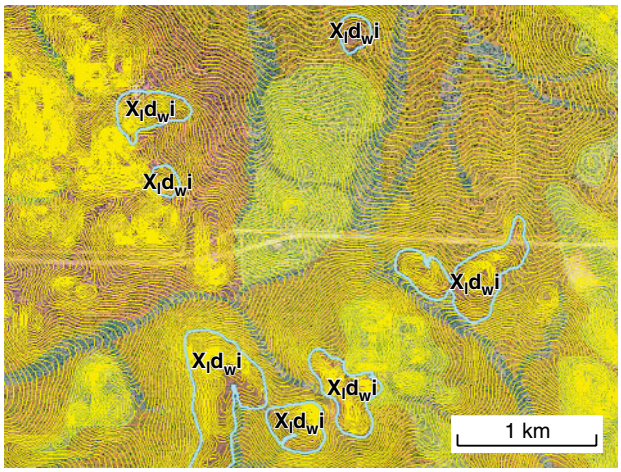

MSS65 30.05.05

Figure 3.15. Ferruginized saprolite — orthophotographic image overlain by ferruginized saprolite polygons ($X_l d_w i$) on hill crests. The central point of the image is 375515E 6597920N

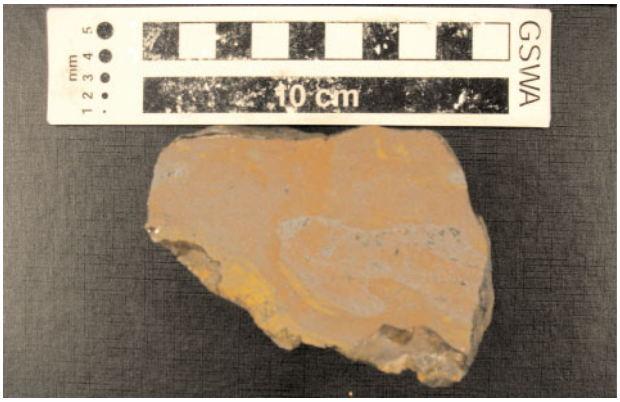

MSS68 30.05.05

Figure 3.16 Massive ferruginized saprolite. Sample site 256023 (376370E 6591900N)

MSS66 30.05.05

Figure 3.17 Outcrop of silicified and ferruginized saprolite on low rise. Sample site 256790 (380655E 6623950N)

MSS67 30.05.05

Figure 3.18 Close-up of outcrop of silicified and ferruginized saprolite. Sample site 256790; length of pen is 13.5 cm

Exposed (X) (cont.)

Xq Quartz vein and surrounding rubble Figures 3.19–3.20

Occurrence: in colluvial–relict domains, including rejuvenated pediment.

Topographic setting: on low rises and hills, where outcrops are common.

Regolith materials: quartz rubble surrounding quartz vein outcrops; may include lithological lag derived from host rocks to the quartz veining.

Database code: _X-q

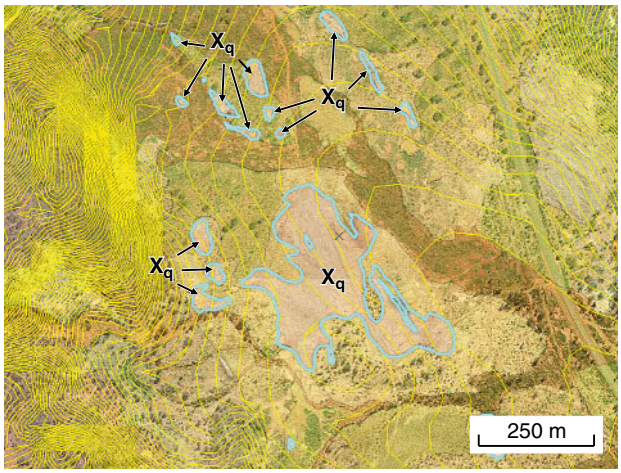

MSS16 30.05.05

Figure 3.19. Quartz vein and surrounding rubble — orthophotographic image overlain by quartz vein and surrounding quartz rubble polygons (*Xq*). The central point of the image is 356200E 6586280N

MSS69 30.05.05

Figure 3.20. Quartz vein with surrounding quartz rubble. Sample site 255826, looking north (345415E 6623505N)

Colluvial (C)

C_a Colluvial fan

Figure 3.21

Occurrence: accumulation of material eroded from hills; proximal

Topographic setting: on lower valley slopes.

Regolith materials: sand and clay; detritus from hinterland.

Database code: _Ca

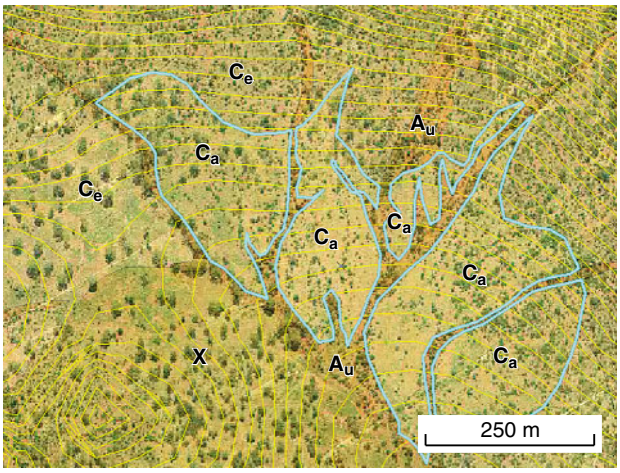

Figure 3.21. Colluvial fan — orthophotographic image overlain by colluvial fan polygons (C_a), cut by drainages (A_u), and surrounded by pediment (C_e) and a hill or rise with outcrop (*X*). The central point of the image is 360240E 6599000N

Colluvial (C) (cont.)

C_e Pediment — Figures 3.22–3.24

Occurrence: the dominant landform on the map, surrounding areas of outcrop and rimmed by a zone transitional to alluvial plain, playas, and eolian sandplain.

Topographic setting: gently sloping, generally flat, downslope from hills, with a veneer of locally derived detritus; locally, however, this veneer may be alluvial or eolian towards the outer margins of the unit, or around internal units of alluvial plain.

Regolith materials: variable, from sandy clays with sparse lag to ferruginous soils with abundant lag; soils are commonly calcareous, and may contain calcrete horizons at shallow (~0.1–0.3 m) depth.

Database code: _Ce

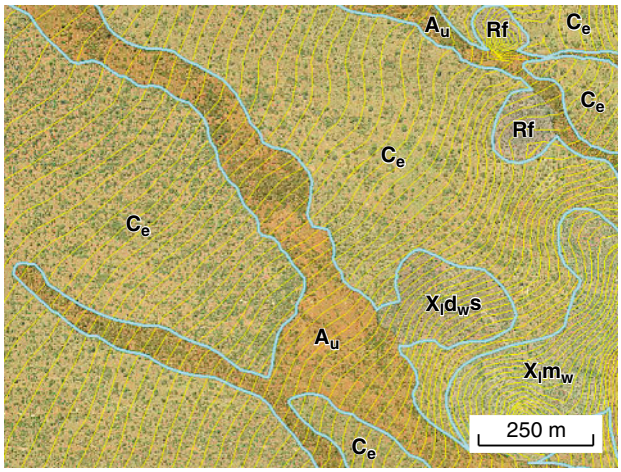

MSS28 30.05.05

Figure 3.22. Pediment — orthophotographic image overlain by pediment polygons (C_e) surrounding hills or rises with outcrops of ferruginous material (*Rf*), weathered mafic rock ($X_l m_w$) and weathered metasedimentary rock ($X_l d_w s$), and cut by drainages (A_u). The central point of the image is 372465E 6601400N

MSS12 30.05.05

Figure 3.23. General view of pediment on gentle slope. Sample site 257253, looking south (376890E 6509055N)

MSS49 30.05.05

Figure 3.24. Coarse-grained ferrolithic and fine-grained quartz and pisoid lag on surface of pediment. Sample site 257253; length of pen is 13.5 cm

Colluvial (C) (cont.)

C_ef Pediment derived from erosion of cemented ferruginous gravel

Figure 3.25

Occurrence: surrounding significant outcrops of cemented ferruginous gravel.

Topographic setting: on slopes below cemented ferruginous-gravel outcrops on crests of hills.

Regolith materials: ferruginous soils with abundant ferruginous detritus.

Database code: _Ce-f

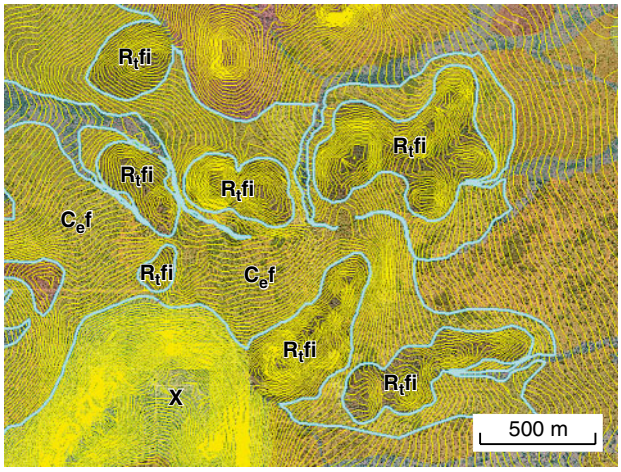

Figure 3.25. Pediment derived from erosion of cemented ferruginous gravel — orthophotographic image overlain by pediment polygons (*C_ef*) surrounding hills and ridges with outcrops of cemented ferruginous gravel (*$R_t$fi*) and bedrock (*X*). The central point of the image is 378790E 6603780N

Colluvial (C) (cont.)

C_j Rejuvenated pediment — Figures 3.26–3.27

Occurrence: new erosion surfaces cut into existing peneplain (pediment), commonly close to the outer margins of the pediment; may be partly associated with westward migration of playas; commonly bounded by breakaways.

Topographic setting: generally flat plains; areas of outcrop at the margins (or even internally).

Regolith materials: thin colluvial-surface horizon (commonly <1 m) overlying saprolite; alluvial or eolian material may be present locally.

Database code: _Cj

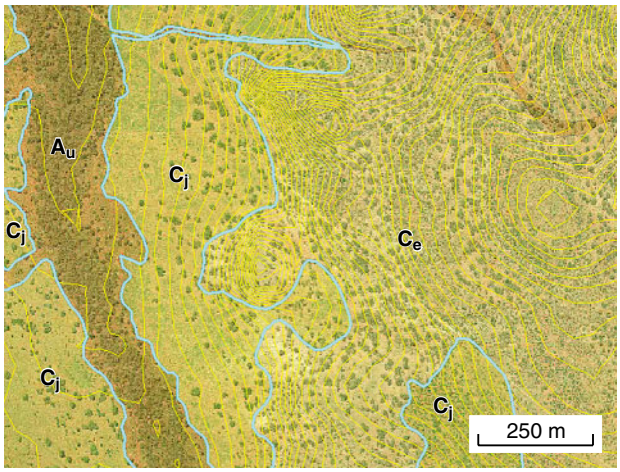

MSS51 30.05.05

Figure 3.26. Rejuvenated pediment — orthophotographic image overlain by rejuvenated pediment polygons (C_j) cut into older pediment (C_e) and cut by drainages (A_u). The central point of the image is 370425E 6609900N

MSS52 30.05.05

Figure 3.27. Rejuvenated pediment (thin layer (<0.5 m) of eolian material overlying saprolite) in the foreground with bounding breakaway in the background; near Binduli, looking north (347735E 6588565N)

Low-gradient slope (W)

W_e Transitional zone between pediment and areas of thick transported regolith — Figure 3.28

Occurrence: a zone along the outer margin between pediment and the eolian–playa domain; variable thickness of transported cover (up to 25 m, as determined from drillhole logs); distal.

Topographic setting: flat, gently sloping, may contain isolated low rises or hills with outcrop.

Regolith materials: somewhat variable, from pale orange-brown calcareous soil with sparse calcrete, quartz with or without ferruginous pisoid lag, to tan soil with abundant ferruginous pisoid lag.

Database code: _We

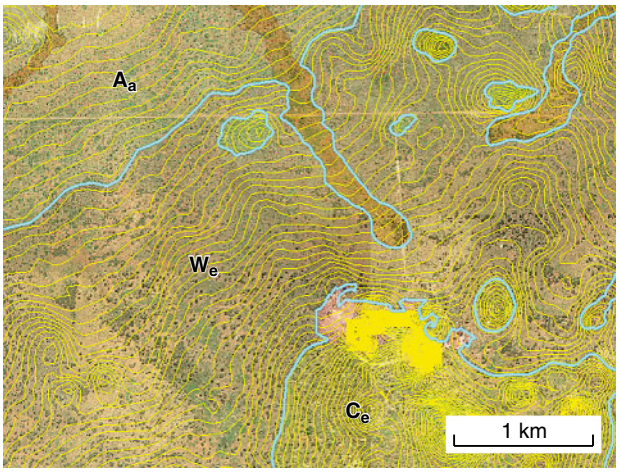

MSS53 30.05.05

Figure 3.28. Transitional zone between pediment and areas of transported regolith — orthophotographic image overlain by transitional zone polygon (W_e) between alluvial plain (A_a) and pediment (C_e) with low hills and rises with outcrop. The central point of the image is 359185E 6616700N

Alluvial (A)

A_a Alluvial plain — Figures 3.29–3.32

Occurrence: forms a fringing zone around the transitional zone to pediment, and as shallow depositional basins within pediment.

Topographic setting: flat, gently sloping terrain, cut by drainages.

Regolith materials: vary considerably, from pale orange-brown sandy clay (with locally developed lag), to tan ferruginous soils with abundant fine-grained, ferruginous, pisoid lag; soil profiles may contain nodular calcrete, either at surface or at shallow depth (<0.1–0.3 m), and ferruginous gravels.

Comments: on Landsat images (band ratios 5/7:4/7:4/2 on red:green:blue), the signal from the surface is generally masked by tall trees (white on the image); this feature, although not diagnostic, can be used to aid discrimination between alluvial plain and eolian sandplain (Fig. 3.30).

Database code: _Aa

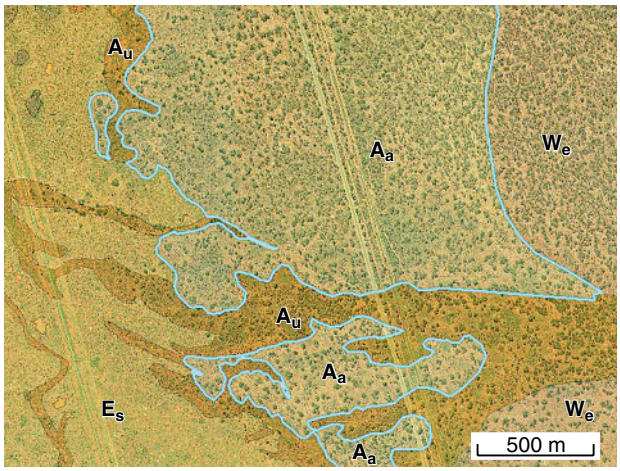

MSS6 30.05.05

Figure 3.29. Alluvial plain — orthophotographic image overlain by alluvial plain polygons (A_a). The polygons lie between eolian sandplain (E_s) to the west and transition zone (W_e) to the east, and are cut by drainages (A_u). The central point of the image is 351410E 6610130N

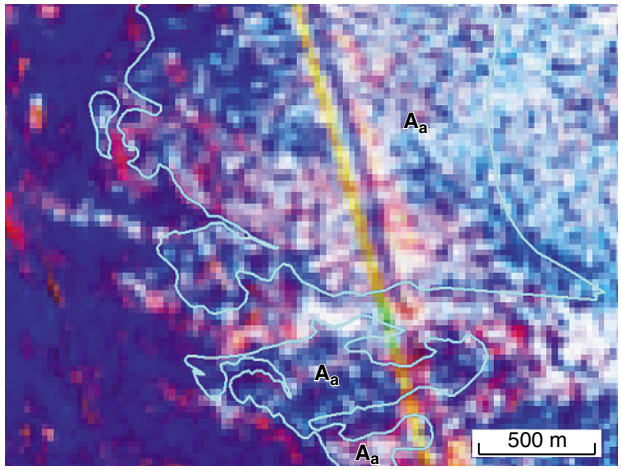

MSS29 30.05.05

Figure 3.30. Landsat image (band ratios 5/7:4/7:4/2 on red: green:blue) with superimposed alluvial plain polygons (A_a). White reflects vegetation — on the alluvial plain, in the transitional zone, and in the drainages. Note the contrast with eolian plain to the west. The central point of the image is 351410E 6610130N

MSS30 30.05.05

Figure 3.31. General view of alluvial plain. Sample site 255965, looking northwest (351700E 6610050N)

MSS31 30.05.05

Figure 3.32. Alluvial plain, showing pale orange-brown sandy clay with sparse, fine-grained quartz and ferruginous pisoid lag. The length of the pen is 13.5 cm

Alluvial (A) (cont.)

A_c Stream channel Figure 3.33

Occurrence: most commonly as narrow drainage lines incised into hilly terrain, as tributaries to larger drainages.

Topographic setting: commonly in hilly terrain, but may occur in most landform settings.

Regolith materials: in channels draining hilly terrain, poorly sorted sediment ranging from sand to boulders; in flat terrain, generally sand and clay, but may also include pebble-sized detritus.

Database code: _Ac

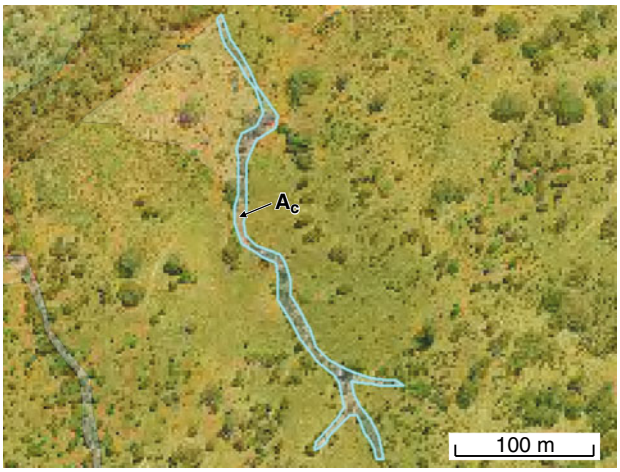

Figure 3.33. Stream channel — orthophotographic image overlain by stream channel polygon (A_c). The channel drains into a larger drainage (A_u) in the northwest corner. The central point of the image is 346815E 6584180N

Alluvial (A) (cont.)

A_d Drainage depression — Figures 3.34–3.35

Occurrence: mainly in the eolian–playa domain, as linear drainages between dune sands, connecting playas

Topographic setting: flat to gently undulating; some incision of the drainages may occur, with steep to vertical banks up to 0.5 m in height.

Regolith materials: typically eolian sand; where saprolite outcrops in the drainages, detritus derived from the saprolite may lie along the bed of the drainage.

Database code: _Ad

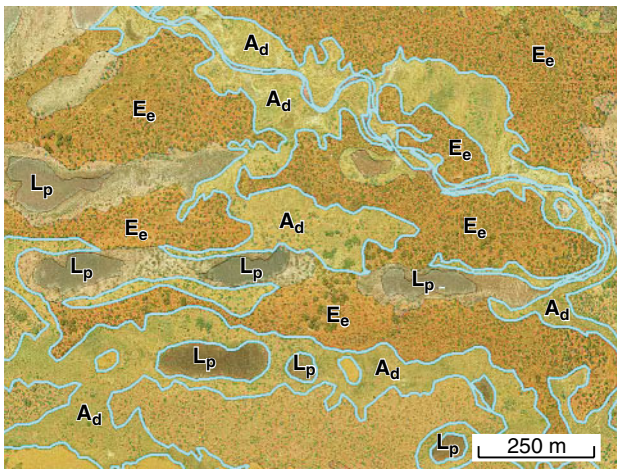

MSS33 30.05.05

Figure 3.34. Network of drainage depressions — orthophotographic image overlain by drainage depression polygons (A_d). Small playas (L_p) either may occur within the depressions or be linked by them. Low sand dunes (E_e) lie between the drainage depressions. The central point of the image is 345790E 6608355N

MSS7 30.05.05

Figure 3.35. Drainage depression in eolian sandplain with low banks and weathered granitic outcrop. Sample site 255921, looking west (349200E 6622560N)

Alluvial (A) (cont.)

A_e Delta

Figure 3.36

Occurrence: at playa margins.

Topographic setting: flat; some dissection by drainages.

Regolith materials: sand and clay.

Database code: _Ae

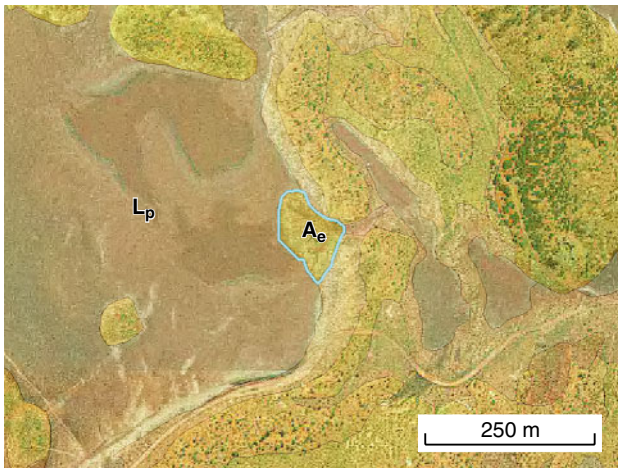

Figure 3.36. Delta — orthophotographic image overlain by delta polygon (A_e). The delta has built up around a drainage inlet to the playa (L_p). The central point of the image is 349565E 6586595N

Alluvial (A) (cont.)

A_pc Claypan — Figures 3.37–3.39

Occurrence: dominantly in eolian–playa domain, in areas peripheral to the playas; generally irregular and typically less than 100 m in diameter.

Topographic setting: flat; eolian sandplain.

Regolith materials: pale orange-brown clay-rich sand; fine-grained lag very rare to absent.

Database code: _Ap-c

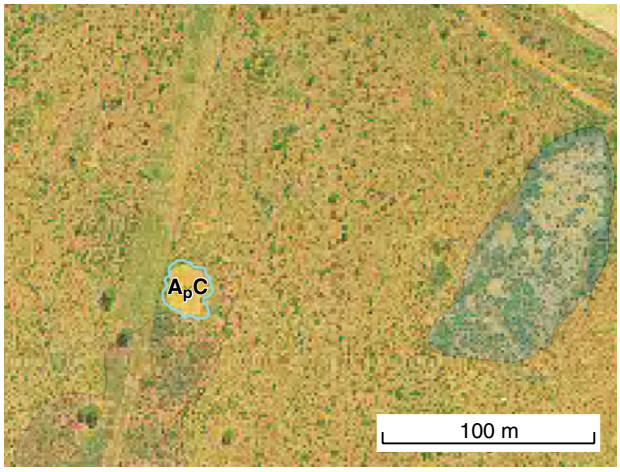

MSS35 30.05.05

Figure 3.37. Claypan — orthophotographic image overlain by claypan polygon (A_pc). The central point of the image is 350650E 6618630N

MSS36 30.05.05

Figure 3.38. Claypan in eolian sandplain. Sample site 255804, looking east (350530E 6618605N)

MSS37 30.05.05

Figure 3.39. Mud cracks on the surface of the claypan. Very rare quartz lag is locally visible. Sample site 255804; the length of the pen is 13.5 cm

Alluvial (A) (cont.)

A_u Drainage channel — Figures 3.40–3.43

Occurrence: subtle depressions draining pediment and alluvial plain and flowing into the playa system; some of the larger drainages also contain alluvium; boundaries of larger superficial drainage channels may be diffuse and merge into areas of active sheetwash.

Topographic setting: ranges from creeks draining hills to subtle depressions in flat to very gently sloping terrain.

Regolith materials: at surface: typically sandy clays; sparse lag (typically quartz with or without ferruginous pisoid); in the subsurface: alternating horizons of sandy clays and gravel (ferruginous, or mixtures of ferruginous gravel with quartz).

Comments: drainage polygons are well-defined on Landsat imagery where vegetation is abundant, but poorly defined where vegetation is relatively sparse (Fig. 3.41).

Database code: _Au

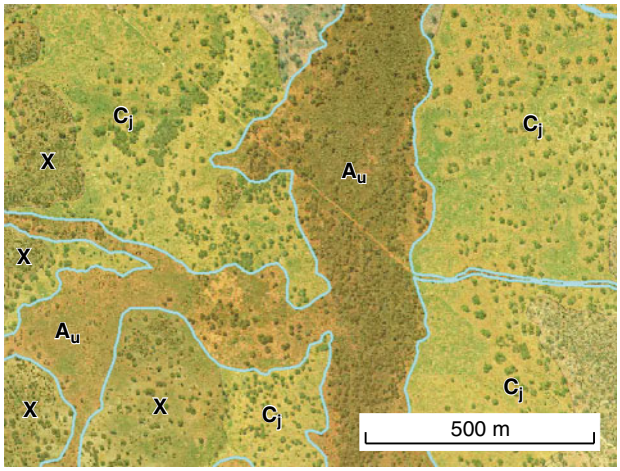

MSS38 30.05.05

Figure 3.40. Drainage — orthophotographic image overlain by drainage polygon (A_u). The drainage cuts rejuvenated pediment (C_j) and low hills or rises with outcrop (X). The central point of the image is 369480E 6610600N

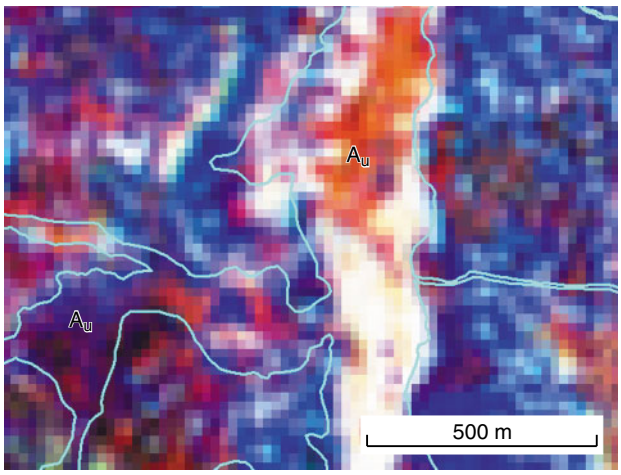

MSS8 30.05.05

Figure 3.41. Landsat image (band ratios 5/7:4/7:4/2 on red:green:blue) with superimposed superficial drainage channel polygon (A_u). White to pale orange-red indicates abundant vegetation (tall trees) along the drainage. The line of drainage is not clearly visible in the Landsat image where there are no trees. The central point of the image is 369480E 6610600N

MSS39 30.05.05

Figure 3.42. Superficial drainage channel. Sample site 257332, looking southeast (369545E 6610670N)

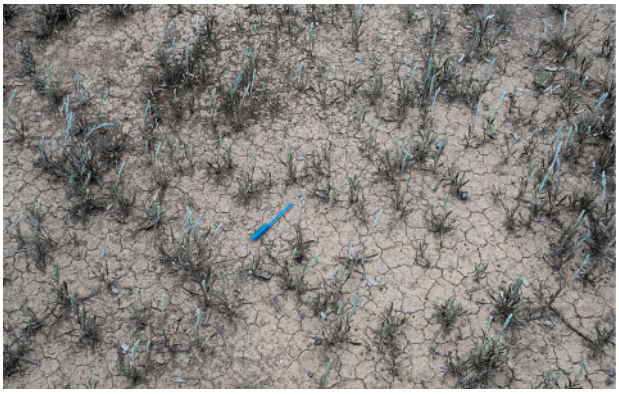

MSS43 30.05.05

Figure 3.43. Mud cracks in sandy clay in drainage. Sample site 257332; length of pen is 13.5 cm

Alluvial (A) (cont.)

A_v Alluvial fan — Figure 3.44

Occurrence: at the interface between the playa system and tributary superficial drainages within alluvial plain.

Topographic setting: flat, very gently sloping terrain at the margins of the playa system.

Regolith materials: sand and clay.

Database code: _Av

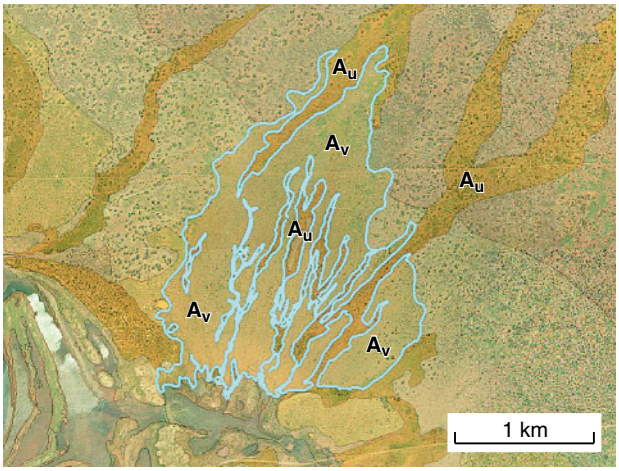

Figure 3.44. Alluvial fan—orthophotographic image overlain by alluvial fan polygons (A_v). Note the anastomosing network of drainages (A_u). The central point of the image is 374660E 6621300N

Alluvial (A) (cont.)

A_y Spherical depression in eolian sandplain — Figure 3.45

Occurrence: spherical depressions commonly in eolian sandplain; commonly boggy after rainfall; commonly associated with claypans; similar in form to claypans and small playas

Topographic setting: flat, gently sloping sandplain.

Regolith materials: sand and clay; differ from playas in containing no evaporitic material.

Database code: _Ay

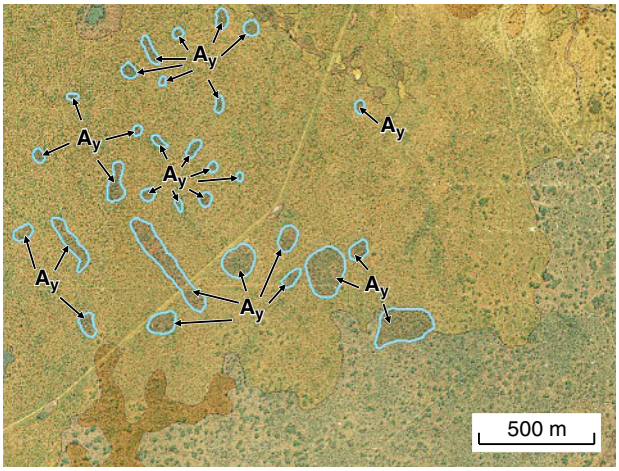

Figure 3.45. Spherical depression in eolian sandplain (E_s) — orthophotographic image overlain by spherical depression polygons (A_y). The central point of the image is 354000E 6619270N

Lacustrine (L)

L_m Playa margin — Figure 3.46

Occurrence: around playas; comprise many components, including beaches and relict dunes; characteristically has a striped pattern (relict dunes), resulting from westward migration of playas.

Topographic setting: gently sloping, locally slightly undulating, terrain around the margins of playas.

Regolith materials: gypsiferous sand and clay; quartz sand lag on some beaches.

Database code: _Lm

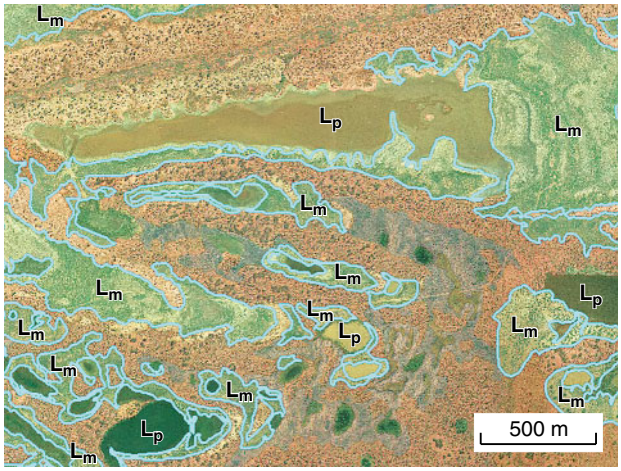

MSS42 30.05.05

Figure 3.46. Playa margins — orthophotographic image overlain by playa margin polygons (L_m) surrounding playas (L_p). The central point of the image is 359355E 6622405N

Lacustrine (L) (cont.)

L_p Playa — Figures 3.47–3.49

Occurrence: in the eolian–playa domain, along the Roe Palaeochannel (including tributaries); relict fluvial system.

Topographic setting: at the lowest points of the topography; effectively drainage sumps.

Regolith materials: ferruginous clays, with gravel (quartz and/or ferruginous) horizons; locally with evaporite (gypsum, halite) crusts.

Database code: _Lp

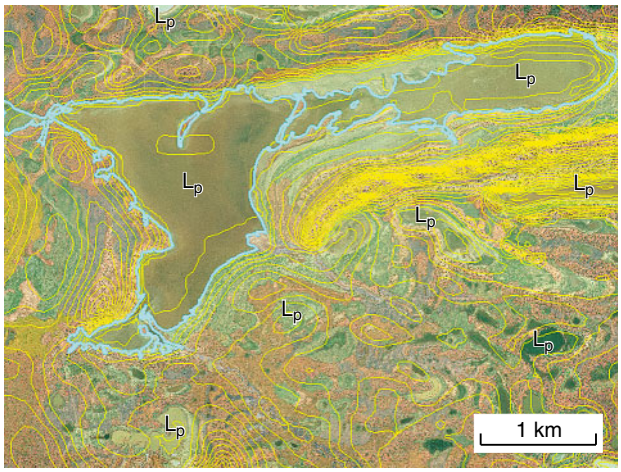

MSS9 30.05.05

Figure 3.47. Playas — orthophotographic image overlain by playa polygons (L_p). The central point of the image is 357225E 6622650N

MSS44 30.05.05

Figure 3.48. Playa. Sample site 255874, looking south (334080E 6615425N)

MSS45 30.05.05

Figure 3.49. Orange-brown sandy-clay playa surface with rare fine-grained quartz and ferruginous pisoid lag. Sample site 255874; length of pen is 13.5 cm

Eolian (E)

E_e Sand dune — Figures 3.50–3.52

Occurrence: in the eolian–playa domain; marginal to, or within, playas and marginal to drainage depressions.

Topographic setting: low, commonly elongate rises.

Regolith materials: sand, typically with iron oxide coatings; rare quartz-sand lag; very rare ferruginous pisoid or silcrete lag.

Database code: _Ee

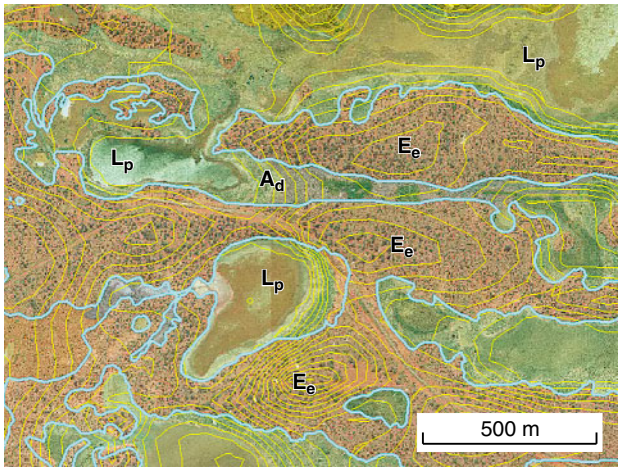

MSS46 30.05.05

Figure 3.50. Sand dunes — orthophotographic image overlain by sand dune polygons (E_e) around playas (L_p) and cut by linear drainage depressions (A_d). The central point of the image is 346460E 6619955N

MSS47 30.05.05

Figure 3.51. Low sand dune. Sample site 255819, looking south (347335E 6614775N)

MSS48 30.05.05

Figure 3.52. Surface of low sand dune, showing sand with rare, very fine grained quartz and silcrete lag. Sample site 255819; length of pen is 13.5 cm

Eolian (E) (cont.)

$E_e e_g$ Gypsiferous sand dune — Figures 3.53–3.55

Occurrence: in the eolian–playa domain; the larger dunes form long (up to 4 km) ridges up to 10 m in height at playa margins.

Topographic setting: low ridges around playa margins.

Regolith materials: gypsiferous plugs, pavements, irregular patches, and crusts in sand dunes; no kopi dunes were identified during the mapping.

Database code: _Ee-eg

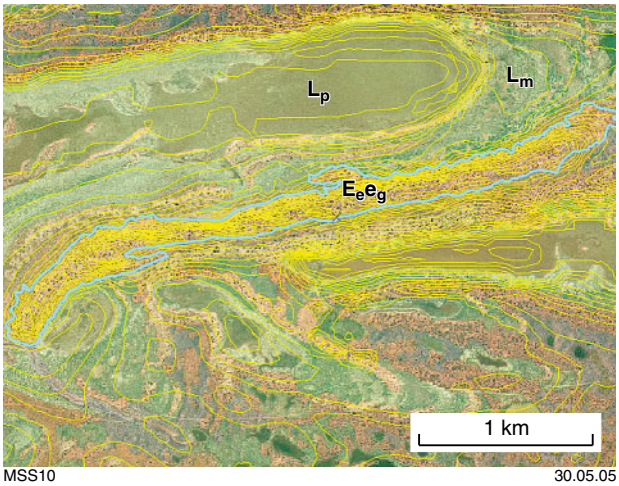

MSS10 30.05.05

Figure 3.53. Gypsiferous sand dune — orthophotographic image overlain by gypsiferous sand-dune polygon ($E_e e_g$) at the edge of a playa (L_p) and its margins (L_m). The central point of the image is 358235E 6623210N

MSS19 30.05.05

Figure 3.54. Footslope of gypsiferous sand dune showing patchy distribution of gypsiferous crusts. Sample site 255795 (347805E 6613265N)

MSS20 30.05.05

Figure 3.55. Gypsiferous crust and rare quartz lag on surface of gypsiferous sand dune. Sample site 255795; length of pen is 13.5 cm

Eolian (E) (cont.)

E_pe_g Gypsiferous sand sheet — Figure 3.56

Occurrence: in the vicinity of playas; some of these may either be degraded dunes, or dunes in their early stage of formation; the sheets can be distinguished from dunes by their low height (<2 m) above the local land surface.

Topographic setting: in the lowest points of the topography associated with playas.

Regolith materials: gypsiferous sand and clay.

Database code: _Ep-eg

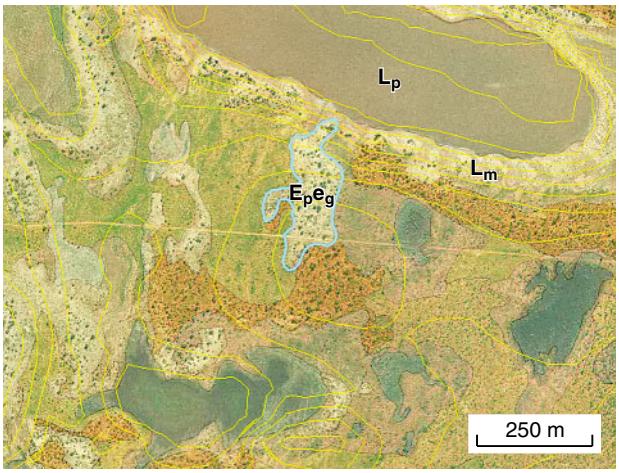

MSS21 30.05.05

Figure 3.56. Gypsiferous sand sheet — orthophotographic image overlain by gypsiferous sand sheet polygon (E_pe_g) at the edge of a playa (L_p) and its margins (L_m). The central point of the image is 362350E 6622985N

Eolian (E) (cont.)

E_s Eolian sandplain overlying alluvial–playa plain Figures 3.57–3.60

Occurrence: in the eolian–playa domain, peripheral to the playa–dune systems and marginal to alluvial plain.

Topographic setting: flat, gently sloping sandplain, forming a generally thin layer (commonly <2 m thick) over alluvial material.

Regolith materials: sand with minor clay; commonly with coarse quartz-sand lag.

Comments: compared to adjacent alluvial plain, this unit is characterized by a lack of tall vegetation, and consequently the general boundary between these two units on Landsat imagery is distinct (Fig. 3.58).

Database code: _Es

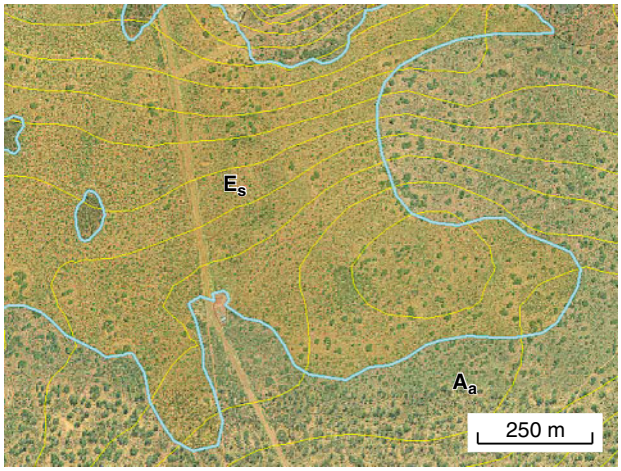

MSS22 30.05.05

Figure 3.57. Eolian sandplain — orthophotographic image overlain by eolian sandplain polygon (E_s) in contact with alluvial plain (A_a). The central point of the image is 365110E 6621515N

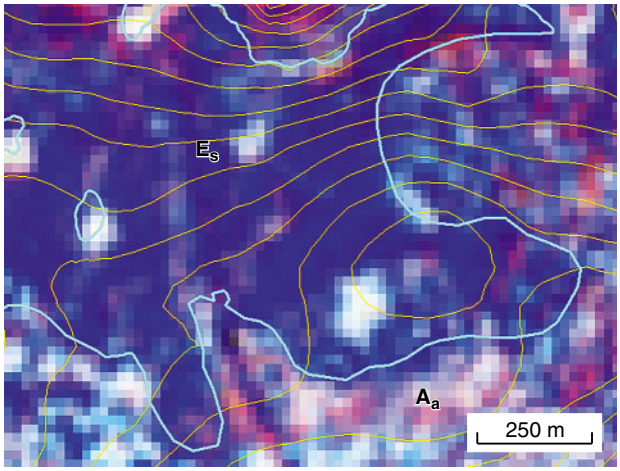

MSS23 30.05.05

Figure 3.58. Landsat image (band ratios 5/7:4/7:4/2 on red:green:blue) with superimposed eolian sandplain polygon (E_s) showing contrast with alluvial plain (A_a). The central point of the image is 365110E 6621515N

MSS11 30.05.05

Figure 3.59. Eolian sandplain. Sample site 255789, looking south (349045E 6613330N)

MSS24 30.05.05

Figure 3.60. Surface of eolian sandplain, with slightly more clay-rich patches raised above sandier areas. A fine lag of relatively coarse, white quartz sand is visible in the latter. Sample site 255789; length of pen is 13.5 cm

Eolian (E) (cont.)

E_w Swale

Figure 3.61

Occurrence: linear to curvilinear depressions in eolian sandplain or between dunes.

Topographic setting: low points in the landscape.

Regolith materials: sand and clay.

Database code: _Ew

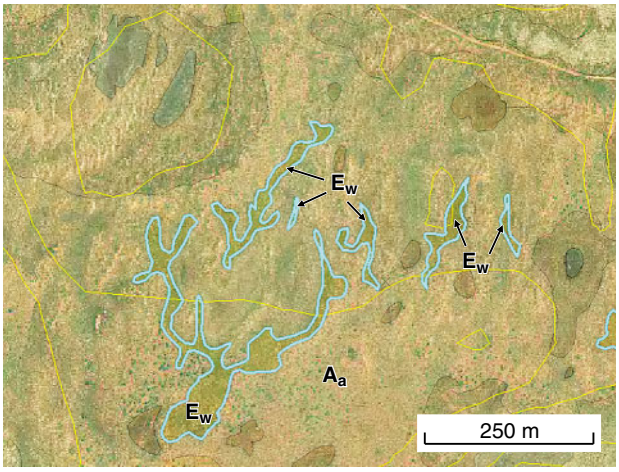

Figure 3.61. Swales in alluvial plain (A_a) — orthophotographic image overlain by swale polygons (E_w). The central point of the image is 351075E 6621700N

Sandplain (S)

S Sandplain Figure 3.62

Occurrence: a mantle of eolian sand over pediment; it differs from eolian sandplain in that it supports taller vegetation and contains calcrete horizons.

Topographic setting: valleys and rises or hills, mirroring underlying topography.

Regolith materials: pale orange-brown, calcareous sandy clays with minor lag: calcrete; quartz; ferruginous pisoid.

Database code: _S

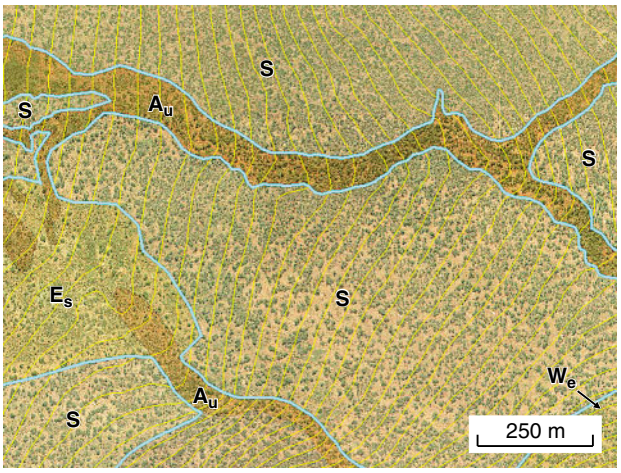

Figure 3.62. Sandplain — orthophotographic image overlain by sandplain polygons (*S*).The sandplain is cut by drainages (*A_u*) and sits between eolian sandplain (*E_s*) and the transitional zone (*W_e*). The central point of the image is 346560E 6598565N

SKWARNECKI

Regolith–landform mapping and hyperspectral data for the Kalgoorlie–Kanowna area

RECORD 2005/7

This Record is published in digital format (PDF) as part of a digital dataset on DVD. It is also available online at: www.doir.wa.gov.au/gswa/onlinepublications. Laser-printed copies can be ordered from the Information Centre for the cost of printing and binding.

Further details of geological publications and maps produced by the Geological Survey of Western Australia can be obtained by contacting:

Information Centre
Department of Industry and Resources
100 Plain Street
East Perth WA 6004
Phone: (08) 9222 3459 Fax: (08) 9222 3444

www.doir.wa.gov.au/gswa/onlinepublications